Performance Analysis of Device-to-Device Communications with Dynamic Interference Using Stochastic Petri Nets

Lei Lei, *Member, IEEE*, Yingkai Zhang, Xuemin (Sherman) Shen, *Fellow, IEEE*, Chuang Lin, *Senior Member, IEEE*, and Zhangdui Zhong

***Abstract*—In this paper, we study the performance of Device-to-Device (D2D) communications with dynamic interference. In specific, we analyze the performance of frequency reuse among D2D links with dynamic data arrival setting. We first consider the arrival and departure processes of packets in a non-saturated buffer, which result in varying interference on a link based on the change of its backlogged state. The packet-level system behavior is then represented by a coupled processor queuing model, where the service rate varies with time due to both the fast fading and the dynamic interference effects. In order to analyze the queuing model, we formulate it as a Discrete Time Markov Chain (DTMC) and compute its steady-state distribution. Since the state space of the DTMC grows exponentially with the number of D2D links, we use the model decomposition and some iteration techniques in Stochastic Petri Nets (SPNs) to derive its approximate steady state solution, which is used to obtain the approximate performance metrics of the D2D communications in terms of average queue length, mean throughput, average packet delay and packet dropping probability of each link. Simulations are performed to verify the analytical results under different traffic loads and interference conditions.**

***Index Terms*—Device-to-device communication; performance analysis; coupled processor model; stochastic petri nets.**

I. Introduction

DEVICE-TO-DEVICE (D2D) communications are commonly referred to as the type of the technologies that enable devices to communicate directly with each other without the infrastructure, e.g, access points or base stations. Bluetooth and WiFi-Direct are two most popular D2D techniques in the market, bothing working in the unlicensed 2.4 GHz ISM bands. Cellular networks, on the other hand, do not support direct over-the-air communications between user devices. However, with the emergence of context-aware applications and the accelerating growth of Machine-to-Machine (M2M) applications, D2D function plays a more and more important role since it facilitates the discovery of geographically close devices and reduce the communication cost between these devices. To seize the emerging market that requires D2D function, the mobile operators and vendors are exploring the possibilities of introducing D2D function in the cellular networks to develop the network assisted D2D communications technologies [1]–[4]. The most significant difference between the cellular network assisted D2D communications and the traditional D2D technologies such as WiFi-direct is that the former works in the licensed band of cellular networks with more controllable interference and the base station or the network can assist the D2D user equipments (UEs) in various functions, such as new peer discovery methods, physical layer procedures, and radio resource management algorithms.

In the emerging new cellular networks such as 3rd Generation Partnership Project (3GPP) Long Term Evolution (LTE), orthogonal time-frequency resources are allocated to different users within a cell to eliminate intracell interference. The introduction of D2D function may bring two categories of potential intracell interference into cellular networks: interference between different D2D users and interference between a cellular user and one or multiple D2D users. The former category of interference arises when the radio resources are reused by multiple D2D users, while the latter arises when the radio resources allocated to a cellular user are reused by one or more D2D users. The latter category of interference can be avoided by statically or semi-statically allocating a group of dedicated resources to all the D2D users at the cost of reduced spectrum efficiency. Most of the existing work on D2D communications focus on the design of optimized resource management algorithms using a static interference model, where each D2D link or cellular link is assumed to be saturated with infinite backlogs and constantly cause interference to the other D2D links or cellular links [5]–[11]. The base station can either centrally determine the radio resource allocation of D2D connections along with the cellular connections [4], [5] or let the users perform distributed resource allocation by themselves [3], [6]. In this paper, we focus on the first category of interference (i.e., interference between D2D links)

Manuscript received December 31, 2012; revised March 17 and June 24, 2013; accepted September 18, 2013. The associate editor coordinating the review of this paper and approving it for publication was C.-F. Chiasserini.

This work was supported by the National Basic Research Program of China (973 program: 2010CB328105), the National Natural Science Foundation of China (No. 61272168, No.60932003), the Fundamental Research Funds for the Central Universities (No. 2012JBM003, No. 2010JBZ008), the State Key Laboratory of Rail Traffic Control and Safety (Contract No. RCS2011ZT005), Beijing Jiaotong University.

L. Lei and Z. Zhong are with the State Key Laboratory of Rail Traffic Control and Safety, Beijing Jiaotong University, China.

Y. Zhang is with the Wireless Signal Processing and Network (WSPN) Lab, Beijing University of Posts & Telecommunications, China.

X. Shen is with the Department of Electrical and Computer Engineering, University of Waterloo, Waterloo, Ontario, Canada (e-mail: xshen@bbcr.uwaterloo.ca).

C. Lin is with the Department of Computer Science and Technology, Tsinghua University, Beijing, China.

Digital Object Identifier 10.1109/TWC.2013.101613.122076

with centralized resource allocation and study the performance of D2D communications using a dynamic interference model, where the finite amount of data arrives to the links at each time slot. Thus, the links do not always have data to transmit and cause interference to the other links. In order to focus on the dynamic interference, we consider the Full Reuse (FR) resource sharing strategy in this paper, where all the available resources are reused by all the D2D links with non-empty queues in each time slot.

In the queuing model for such system, the service rate at each queue varies with time due to two factors: the fast fading effect of the wireless channel and the dynamic arrival and departure of packets which results in the dynamic variation of interference from a link when its status changes from busy to idle or vice versa. When only the second factor is considered, the system can be modeled as a coupled-processor server, where the service rates at each queue vary over time as governed by the backlogged state of the other queues. The complex interaction between the various queues renders an exact analysis intractable in general and steady-state queue length distributions are known only for exponentially distributed service in two-queue systems [12]–[14]. In [15], [16], the flow-level performance in wireless networks with multiple base stations is investigated, which can be formulated as a coupled-processor model in the single user class scenario. Due to the complex nature of the coupled-processor model, [15] derives bounds and approximations for the key performance metrics by assuming maximum and minimum interference in neighbours of the reference cell and [16] studies the performance gains of intercell scheduling in a two-cell network and a simplified symmetric network, respectively. In [17], the upper and lower bounds on the moments of the queue length of the coupled-processor model are obtained by formulating a moments problem and solving a semidefinite relaxation of the original problem. This analysis method is applied in [18] to study the impact of user association policies on flow-level performance in interference-limited wireless networks. Although the semidefinite relaxation method can be applied to study the coupled-processor model with more than two queues, the size of the formulated optimization problem scales exponentially as the number of queues increases.

In this paper, we consider both the fast fading and dynamic interference effects to better depict the variations of the service rate in the practical D2D system. The Finite-State Markov Channel (FSMC) model with respect to the Signal to Interference and Noise Ratio (SINR) is constructed for each link, which not only captures the fast fading effect of the wireless channel as in the traditional FSMC model based on Signal to Noise Ratio (SNR) partition [19], [21], but also considers the dynamic variation of interference due to the changing backlogged states of the other active links. Based on the above FSMC model, we formulate a coupled processor queuing model for such a system with time-varying service rates and propose an analytical method to derive the state transition probability matrix and steady-state distribution of the underlying Markov process. However, the scalability of proposed analytical method with large number of links is limited by the exponentially increasing state space of the Markov process. Therefore, we use the model decomposition and iteration approach in Stochastic Petri Nets (SPN) [22], [23] to deal with the coupling between the service rates of the different links. Specifically, we formulate the SPN model for the above queuing system with multiple D2D links and decompose it into multiple "near-independent" subnets, where each subnet corresponds to a queuing system with a single link and is solved separately. Because the subnets are correlated, after solving the problem in each subnet to get its steady-state statistics, the distributions are exported to other subnets to derive their approximate state transition probability matrices and steady-state distributions, and this is conducted iteratively. Finally, performance metrics such as throughput and packet dropping probability can be obtained from the steady-state distribution of the Markov process.

In recent years, SPN has been used for the performance analysis of wireless networks by some work [24]–[27]. Performance evaluation of resource management has been conducted in cellular networks [25], multihop networks [26], and IEEE 802.16 networks [27] using SPN. In [24], we have used the model decomposition and iteration approach [22], [23] to analyze the performance of opportunistic scheduling in cellular networks. However, the interaction between different subsystems is due to scheduling instead of interference as in this paper. This model decomposition approach has been improved in [28] to deal with the following two potential limits: (1) proofs of convergence are usually difficult to obtain; (2) "spurious" states might be introduced, which do not exist in the exact model. Moreover, [29] eliminates the need for a Kronecker consistent model decomposition. Since our model in this paper is a Kronecker-consistent model, and we can prove the convergence of the fixed-point iteration while no "spurious" states are introduced due to the decomposition, we stick to the decomposition method in [22], [23] due to its simplicity. To the best of our knowledge, this work is the first one which addresses the problem of subnets interaction due to dynamic interference in D2D communications.

In [30], the performance of D2D communications in cellular networks with dynamic packet arrivals is analyzed using SPN. However, the transition probabilities of the channel states under dynamic interference are obtained by Monte-Carlo simulation due to the computation complexity of the numerical method. We extend the work by developing an analytical approach based on level crossing rate of the wireless channel to derive the transition probabilities of the channel states, which greatly reduce the computation complexity. Moreover, we perform extensive numerical analysis and simulation with varying number of D2D links to evaluate the performance metrics such as throughput, delay and dropping probability. In addition, we also consider the Batch Bernoulli arrival process.

The remainder of the paper is organized as follows. In Section II, the system model of D2D communications is first introduced, followed by the formulation of a coupled processor queuing model based on the system model. In Section III, the transition probabilities of the Markov process underlying the queuing model are analyzed in order to derive the steady-state probabilities. In Section IV, we formulate the corresponding SPN model, and use the model decomposition and iteration method in SPN to approximate the system performance. The analytical results are verified by simulation under different

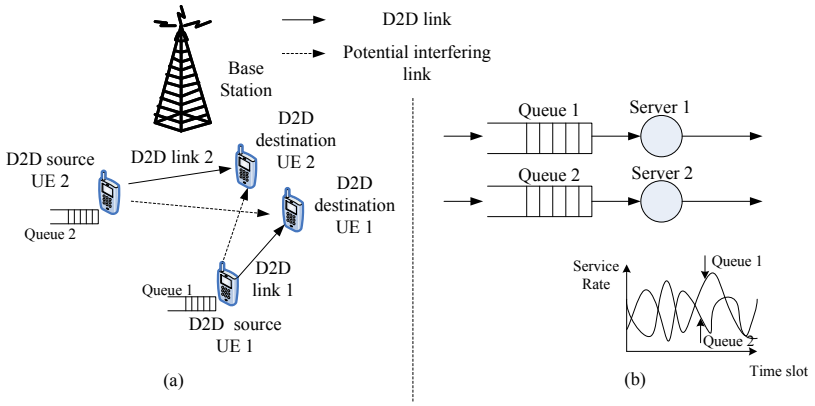

Fig. 1. Cellular wireless networks with D2D communications capability (a) resource sharing between two D2D links; (b) queuing model of (a).

traffic loads and interference conditions in Section V. Finally, conclusion is given in Section VI. As many symbols are used in this paper, Table I summarizes the important ones.

II. The Coupled Processor Queueing System

Consider a cellular wireless network with D2D communication capability. Fig.1(a) illustrates the case where two D2D links share radio resources with each other. A D2D link consists of a source D2D UE transmitting to its destination D2D UE. Potential interfering link exists for D2D link 1 (resp. D2D link 2) from the transmitter of source D2D UE2 (resp. source D2D UE1) to the receiver of destination D2D UE1 (resp. destination D2D UE2). Since there are two categories of links, i.e., D2D links and potential interfering links, all links mentioned are referred to the D2D links by default in the rest of the paper. We consider that each source D2D UE maintains a queue with finite capacity to buffer the dynamically arriving data. An interfering link is 'potential' since it only exists when the queue of the source D2D UE associated with its transmitter is non-empty. The transmission rate of each link is determined by its own SINR, which varies with time due to the fast fading effects of its own wireless channel, and also the fast fading effects and changing on-off status of its potential interfering link. Moreover, the transmission rates of different links vary asynchronously over time. Therefore, Fig.1(a) can be modeled as a queuing system as illustrated in Fig.1(b), where there are two queues and each one is served by a private single-server, whose service rate is determined by the transmission rate of the corresponding link.

Let $\mathcal{D} = 1, \ldots, D$ denote the set of non-overlapping links. Each link maintains a queue at the source D2D UE, and each queue has a finite capacity of $K < \infty$ packets, where packets are assumed to be of the same size B bits. For each queue i, packets arrives according to Poisson distribution with average rate λ_i packets/sec. The transmission in the time is slot-by-slot based and each slot has an equal length ΔT. In each time slot, the resource can be allocated to one or more links, depending on the resource sharing and scheduling strategies. Although there are various resource sharing strategies between the links, there are two extreme cases which incur the maximum and minimum interference, respectively:

- Full Reuse (FR): The links reuse all the available resources, causing interference to each other. However, the links get the largest amount of resources to use.
- Orthogonal Sharing (OS): The links use orthogonal resources with each other where no interference exists. However, each link gets the least amount of resources to use.

In this paper, we focus on the performance of FR strategy with dynamic interference. This resource sharing strategy is not a practical one, since it may cause excessive amount of interference between D2D links. However, it is an extreme case which incurs the maximum interference but achieves the best frequency reuse. On the other hand, the queuing performance of the other extreme case, i.e., the OS strategy, can be analyzed using the method in our earlier work [24]. Since the practical resource allocation strategies try to achieve the best tradeoff between frequency reuse and interference control, the performance of the two extreme cases provide lower bounds for the performance of practical resource allocation strategies. Moreover, the packet-level performance evaluation method of other practical resource allocation methods can be developed based on those of FR and OS strategies.

Assume that the instantaneous channel gains of the D transmitters Tx_i on the source D2D UEs of links $i \in \mathcal{D}$ with the D receivers Rx_j on the destination D2D UEs of links $j \in \mathcal{D}$ remain constant within a time slot, the value of which at time slot t can be represented by a D-by-D channel gain matrix $\mathbf{G}_t$, where item $G_{ij,t}$ denotes the channel gain between the transmitter Tx_i of link i and the receiver Rx_j of link j. The channel gain matrices $\mathbf{G}_t$ and $\mathbf{G}_{t'}$ in different time slots $t \neq t'$ can be different due to the fast fading effects of the wireless channel. Let $\mathcal{I}_i := \{I_{ji}\}_{j \in \mathcal{D} \backslash \{i\}}$ denote the set of potential interfering links of link i, where I_{ji} is the potential interfering link from the transmitter of link $j \in \mathcal{D} \backslash \{i\}$ to the receiver of link i. Note that the channel gain of link i is $G_{ii,t}$, while the channel gains of set of potential interfering links $\mathcal{I}_i$ are $\{G_{ji,t}\}_{j \in \mathcal{D} \backslash \{i\}}$. Let $\mathbf{P} = \{P_i\}_{i=1,\ldots,D}$ be the D-by-1 power matrix that determines the transmission power of every link i.

In this paper, we assume that a link does not always have data to transmit, and its transmitter first examines whether the queue is empty or not at the beginning of every time slot t. Only when the queue is non-empty shall it move the packets out of the queue for transmission and thus cause interference to

TABLE I
SUMMARY OF IMPORTANT NOTATIONS

Category	Symbol	Definition
Constant	D	The number of D2D links
	K	The buffer (queue) capacity in terms of packets
	B	Packet length
	ΔT	Time slot duration
	L	The number of channel states of a single D2D link in FSMC
	χ_l	The SINR threshold between the l-th state and $(l+1)$-th state of a D2D link in FSMC
	R_l	The transmission rate of any D2D link in the l-th state of the FSMC model
Set	$\mathcal{D}$	The set of D2D links i, $i = 1, \ldots, D$
	$\mathcal{I}_i$	The set of potential interfering links of D2D link i
	$\mathcal{J}_{i,t}$	The subset of D2D links excluding link i with non-zero queue length at the beginning of time slot t
Variable	λ_i	The mean packet arrival rate of the Poisson arrival process of D2D link i
	I_{ji}	The potential interfering link from the transmitter of D2D link j to the receiver of D2D link i where j is other than i
	$r_{i,t}$	The instantaneous data rate of D2D link i at time slot t
	$Q_{i,t}$	The queue length of D2D link i at the beginning of time slot t
	$\Theta_{i,t}$	The queue status (empty or non-empty) of the D2D link i at the beginning of time slot t
	$SINR_{i,t}$	The SINR value for each D2D link i at time slot t
	$\gamma_{ii,t}$	The SNR value of D2D link i at time slot t
	$\gamma_{ji,t}$	The virtual SNR value of potential interfering I_{ji} at time slot t
	$H_{i,t}$	The channel state of the FSMC model of D2D link i at time slot t
	$A_{i,t}$	The number of packets arrived to link i during time slot t
	$\hat{H}_{i,t+1}$	The virtual channel state of the FSMC model of D2D link i at time slot $t+1$, which assumes that the queue status of all the other links $j \in \mathcal{D}\backslash\{i\}$ is the same at time slots t and $t+1$
Vector	$\vec{Q}_t$	D-dimensional, where the ith element is $Q_{i,t}$, $i = 1, \ldots, D$
	$\vec{\Theta}_t$	D-dimensional, where the ith element is $\Theta_{i,t}$, $i = 1, \ldots, D$
	$\vec{H}_t$	D-dimensional, where the ith element is $H_{i,t}$, $i = 1, \ldots, D$
	$\vec{\gamma}_{i,t}$	D-dimensional, where the jth element is $\gamma_{ji,t}$, $j = 1, \ldots, D$
Probability	$p^{(\vec{n},\vec{h})}_{(\vec{l},\vec{k})}$	$\Pr.\{\vec{Q}_{t+1} = \vec{h}, \vec{H}_{t+1} = \vec{n} \vert \vec{H}_t = \vec{l}, \vec{Q}_t = \vec{k}\}$
	$p^{\vec{h}}_{(\vec{l},\vec{k})}$	$\Pr.\{\vec{Q}_{t+1} = \vec{h} \vert \vec{H}_t = \vec{l}, \vec{Q}_t = \vec{k}\}$
	$p^{\vec{n}}_{(\vec{l},\vec{k},\vec{h})}$	$\Pr.\{\vec{H}_{t+1} = \vec{n} \vert \vec{H}_t = \vec{l}, \vec{Q}_t = \vec{k}, \vec{Q}_{t+1} = \vec{h}\}$
	$p^{h_i}_{l_i,k_i}$	$\Pr.\{Q_{i,t+1} = h_i \vert H_{i,t} = l_i, Q_{i,t} = k_i\}$
	$p^{n_i}_{(l_i,\vec{k},\vec{h})}$	$\Pr.\{H_{i,t+1} = n_i \vert H_{i,t} = l_i, \vec{Q}_t = \vec{k}, \vec{Q}_{t+1} = \vec{h}\}$
	$p^{n_i}_{(l_i,\theta_v,\theta_w)}$	$\Pr.\{H_{i,t+1} = n_i \vert H_{i,t} = l_i, \{\Theta_{j,t}\}_{j\in\mathcal{D}\backslash\{i\}} = \theta_v, \{\Theta_{j,t+1}\}_{j\in\mathcal{D}\backslash\{i\}} = \theta_w\}$
	$p^{(l_i,n_i)}_{(\theta_v,\theta_w)}$	$\Pr.\{H_{i,t} = l_i, H_{i,t+1} = n_i \vert \{\Theta_{j,t}\}_{j\in\mathcal{D}\backslash\{i\}} = \theta_v, \{\Theta_{j,t+1}\}_{j\in\mathcal{D}\backslash\{i\}} = \theta_w\}$
	$\hat{p}^{n_i}_{(l_i,\theta_v,\theta_w)}$	$\Pr.\{H_i(t+1) = n_i \vert \hat{H}_i(t+1) = l_i, \{\hat{\Theta}_{j,t+1}\}_{j\in\mathcal{D}\backslash\{i\}} = \theta_v, \{\Theta_{j,t+1}\}_{j\in\mathcal{D}\backslash\{i\}} = \theta_w\}$
	$\hat{p}^{l_i,n_i}_{(\theta_v,\theta_w)}$	$\Pr.\{\hat{H}_i(t+1) = l_i, H_i(t+1) = n_i \vert \{\hat{\Theta}_{j,t+1}\}_{j\in\mathcal{D}\backslash\{i\}} = \theta_v, \{\Theta_{j,t+1}\}_{j\in\mathcal{D}\backslash\{i\}} = \theta_w\}$
	$\widetilde{p}^{n_i}_{(l_i,k_i,h_i)}$	Approximate probability of $\Pr.\{H_{i,t+1} = n_i \vert H_{i,t} = l_i, Q_{i,t} = k_i, Q_{i,t+1} = h_i\}$
	$\widetilde{p}^{l_i,n_i}_{(k_i,h_i)}$	Approximate probability of $\Pr.\{H_{i,t} = l_i, H_{i,t+1} = n_i \vert Q_{i,t} = k_i, Q_{i,t+1} = h_i\}$
	$p^{l_i}_{\theta_v}$	$\Pr.\{H_{i,t} = l_i \vert \{\Theta_{j,t}\}_{j\in\mathcal{D}\backslash\{i\}} = \theta_v\}$
	$\pi_{\vec{l},\vec{k}}$	Steady state probability, $\lim_{t\to\infty} \Pr.\{\vec{H}_t = \vec{l}, \vec{Q}_t = \vec{k}\}$
	$\pi^i_{l_i,k_i}$	Steady state probability, $\lim_{t\to\infty} \Pr.\{H_{i,t} = l_i, Q_{i,t} = k_i\}$
	π_{k_j,h_j}	Steady state probability, $\lim_{t\to\infty} \Pr.\{Q_{j,t} = k_j, Q_{j,t+1} = h_j\}$
Performance Metrics	$\overline{Q_i}$	The average queue length of link i
	$\overline{T_i}$	The mean throughput in terms of packets/s of link i
	$\overline{D_i}$	The average packet delay of link i
	p^i_{d}	The packet dropping probability of link i

the other links. We consider the transmission capability of link i during time slot t as $\lfloor \frac{r_{i,t}\Delta T}{B} \rfloor$, where $r_{i,t}$ is its instantaneous data rate in terms of bits/s and $\lfloor \cdot \rfloor$ is the integer no bigger than $\cdot$. Here, we assume that if a packet could not be transmitted completely due to time-slot expiration at the end of time-slot t, which can be foreseen at the beginning of this time slot, the entire packet is not transmitted in this time slot but at the next time-slot $(t+1)$. Although a packet can be truncated for transmission in a realistic scenario, for example, by the RLC protocol in the LTE systems, assuming the realistic scenario will make the queue length a real number instead of an integer, which will result in the infinite state space of the Markov chain. Therefore, we make this approximation in our analysis, while keeping the approximation under control by adjust the packet size B. This approximation has also been used in existing work in literature [21], [31], where the service rate is given in terms of packets/s instead of bits/s. If the number of packets in the queue of link i at the beginning of time slot t is less than its transmission capability during time slot t, padding bits shall be transmitted along with the data according to the LTE standard. Arriving packets are placed in the queue throughout the time slot t and can only be transmitted during the next time slot $t+1$. If the queue length reaches the buffer capacity K, the subsequent arriving packets will be dropped. Let $\vec{Q}_t = \{Q_{i,t}\}_{i\in\mathcal{D}}$ denote the queue length of every link i in terms of packets at the beginning of time slot t, and $A_{i,t}$ denote the number of packets arrived to link i during the time slot t, which is a Poisson distributed stationary process with mean $\lambda_i \Delta T$. According to the above assumption, the queuing process evolves following

$$Q_{i,t+1} = \min[K, \max[0, Q_{i,t} - \lfloor \frac{r_{i,t}\Delta T}{B} \rfloor] + A_{i,t}]. \quad (1)$$

From the above discussion, the SINR of every link i depends on the subset of other links in the system with non-zero queue length at the beginning of time slot t, which is denoted as $\mathcal{J}_{i,t}$. Let $\vec{\Theta}_t = \{\Theta_{i,t}\}_{i\in\mathcal{D}}$, where $\Theta_{i,t} = \mathbf{1}(Q_{i,t} > 0)$ denotes the queue status (empty or not) of the link i at the beginning of time slot t. Note that $\vec{\Theta}_t$ can take 2^D possible values $\theta_v, v = 1\ldots, 2^D$. Therefore, we have $\mathcal{J}_{i,t} := \{j \in \mathcal{D}\backslash\{i\} : \Theta_{j,t} = 1\}$. The SINR value for each link i at time slot t is given by the following formula:

$$SINR_{i,t} = \frac{P_i G_{ii,t}}{N_i + \sum_{j\in\mathcal{D}\backslash\{i\}} P_j G_{ji,t}\Theta_{j,t}} = \frac{\gamma_{ii,t}}{1 + \sum_{j\in\mathcal{D}\backslash\{i\}} \gamma_{ji,t}\Theta_{j,t}}, \quad (2)$$

where $\gamma_{ii,t} := \frac{P_i G_{ii,t}}{N_i}$ is the SNR value of link i, and N_i is the noise power on link i. Similarly, $\gamma_{ji,t} := \frac{P_j G_{ji,t}}{N_i},\ j \in \mathcal{D}\backslash\{i\}$ can be referred to as the 'virtual SNR' value of the link I_{ji}, where it is 'virtual' since I_{ji} is an interference link instead of a link and it is in fact the 'interference to noise ratio' considering the physical meaning.

The corresponding instantaneous data rate $r_{i,t}$ is a function of $SINR_{i,t}$. In this paper, we assume that adaptive modulation and coding (AMC) is used, where the SINR values are divided into L non-overlapping consecutive regions and if the SINR value $SINR_{i,t}$ of link i falls within the l-th region $[\chi_{l-1}, \chi_l)$, the corresponding data rate $r_{i,t}$ of link i is a fixed value R_l, i.e., $r_{i,t} = R_l$, if $SINR_{i,t} \in [\chi_{l-1}, \chi_l)$. Table II gives the AMC scheme in 3GPP LTE systems where $L = 16$ [20]. As an example, $l = 2$ if $SINR_{i,t} \in [-4.46\text{dB}, -3.75\text{dB})$, and $R_2 = 213.3$Kbs. Since the AMC function can select the appropriate coding and modulation schemes according to the instantaneous SINR of the wireless channel guaranteeing that the packet error rate is above an acceptable value, we do not consider the transmission errors. Although it is an interesting and challenging research problem to study the transmission errors due to factors such as imperfect Channel State Information (CSI), it is outside the scope of this paper.

TABLE II
SINR THRESHOLD AND RATES

channel state index l	SINR Threshold $\chi_{(l-1)}$ (dB) $\geq$	Rates R_l (Kbs)
2	-4.46	213.3
3	-3.75	328.2
4	-2.55	527.8
5	-1.15	842.2
6	1.75	1227.8
7	3.65	1646.1
8	5.2	2067.2
9	6.1	2679.7
10	7.55	3368.8
11	10.85	3822.7
12	11.55	4651.2
13	12.75	5463.2
14	14.55	6332.8
15	18.15	7161.3
16	19.25	7776.6

In order to achieve AMC, we assume that the BS has knowledge of the channel gain matrix $\mathbf{G}_t$ and the queue status $\vec{\Theta}_t$ of all the D2D links at each time slot t, so that it can determine the modulation and coding schemes for each D2D link with non-empty queues and inform the source and destination D2D UEs with downlink control signaling. Since network assisted D2D communications have not been standardized in 3GPP, there is currently no specific signaling protocols for resource allocations of D2D connections. In [1], we have proposed a candidate signaling procedure.

Since the SINR value $SINR_{i,t}$ of any link $i \in \mathcal{D}$ can be derived according to (2), the wireless channel for each link i can be modeled as a FSMC with total L states, where $H_{i,t}$ represents the channel state of the FSMC model of link i at time slot t. Each state of FSMC corresponds to one non-overlapping consecutive SINR region and a fixed transmission rate determined by the AMC algorithm. From (2), it can be seen that the SINR value $SINR_{i,t}$ and thus the channel state $H_{i,t}$ of link i depends on the SNR value $\gamma_{ii,t}$ of link i and the 'virtual SNR' values $\gamma_{ji,t}$ of its interfering links $I_{ji},\ j \in \mathcal{D}\backslash\{i\}$, and also the queue status $\Theta_{j,t}$ of the links $j \in \mathcal{D}\backslash\{i\}$. For any link $i \in \mathcal{D}$, since both the (virtual) SNR values $\gamma_{ji,t},\ j \in \mathcal{D}$ and the queue status $\Theta_{j,t},\ j \in \mathcal{D}\backslash\{i\}$ remain constant within a time slot t, the SINR value $SINR_{i,t}$ also remains constant within a time slot.

There has been a lot of research on the finite state Markov

modeling of wireless fading channels, where interference is not considered. Compared with these work, our FSMC has two additional complicating factors: (1) the fading of the potential interfering links of link i; (2) the variation of the set of interfering links of link i due to changing backlog status of the other links. For factor (1), the channel gain of an interfering link in time slot t can be considered as only dependent on its channel gain in time slot $t-1$ due to the time correlation as assumed in the existing first-order FSMC models. For factor (2), the queue length of a link at time slot t only depends on its queue length at time slot $t-1$ and the channel state $H_{i,t-1}$ at time slot $t-1$, as will be discussed later and calculated in (4). Therefore, the channel state $H_{i,t}$ of link i at time slot t only depends on the channel gains of link i and its potential interfering links at time slot $t-1$ and the queue length of the other links at time slot $t-1$, which obeys the Markovian property.

The above D2D communications system can be formulated by a coupled processor queuing model as follows. The defined queuing system consists of a finite number, D, of queues indexed by $i = 1, 2, \ldots, D$, each of which has a server i corresponding to a D2D link i. For any i, there is a Poisson distributed packet arrival process with mean $\lambda_i \Delta T$ fixed length packets of B bits, and a finite and discrete-time Markov chain $H_{i,t}$ with total L states representing the evolution of the channel states of D2D link i. Associated with the l-th ($l \in \{1, \ldots, L\}$) state of the FSMC model of any link i is a fixed service rate R_l bits/sec of server i, which is a non-negative integer and the same for all the links. Since the wireless channels vary with time asynchronously for different links, the transitions of the channel states are link dependent and the channel states $H_{i,t}$ and $H_{j,t}$ of any two different links $i \neq j$ at time slot t are not necessarily the same. If at time slot t the queue i is non-empty with $H_{i,t}$ in the l-th state, the queue i is served at a deterministic rate R_l, i.e., the queue is served according to an L-state MMDP. For any link $i \in \mathcal{D}$, since $SINR_{i,t}$ depends on $\{\Theta_{j,t}\}_{j \in \mathcal{D} \setminus \{i\}}$ and thus $\{Q_{j,t}\}_{j \in \mathcal{D} \setminus \{i\}}$, the state of $H_{i,t}$ depends on the set of queues in the system with non-zero queue length, which corresponds to a coupled processor server.

III. Steady-State Solution of the Queueing System

Let $\vec{H}_t := \{H_{i,t}\}_{i \in \mathcal{D}}$ denote the channel states for every link at time slot t. Let $\vec{Q}_t$ as defined in Section II represent the queue states for every link at time slot t. The $(2 \times D)$-dimensional discrete-time Markov chain (DTMC) $\{(\vec{H}_t, \vec{Q}_t), t = 0, 1, ...\}$ can be used to represent the system behavior of the above queuing system. The state number of the DTMC is $((K+1) \times L)^D$, which grows exponentially with the increasing number D of D2D links. In this section, we focus on the derivation method of the exact transition probabilities and steady-state solution of the DTMC and leave the state space explosion problem to the next section, where the model decomposition and iteration method in SPN is used to decompose the DTMC with $((K+1) \times L)^D$ number of states to D DTMCs each with $(K+1) \times L$ number of states. Based on the exact method discussed in this section, the approximate transition probabilities and steady-state solution of the decomposed DTMCs can be derived.

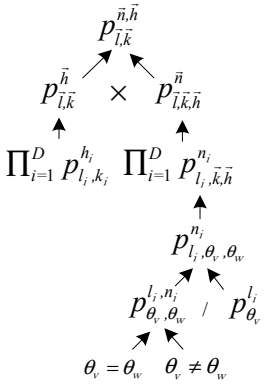

Fig. 2. The computation of $p^{(\vec{n},\vec{h})}_{(\vec{l},\vec{k})}$, which mainly consists of two components. The first component $p^{\vec{h}}_{(\vec{l},\vec{k})}$ represents the transition probability of the queue state, and the second component $p^{\vec{n}}_{(\vec{l},\vec{k},\vec{h})}$ represents the transition probability of the server state.

Let $p^{(\vec{n},\vec{h})}_{(\vec{l},\vec{k})}$ be the transition probability from state $(\vec{l},\vec{k})$ to state $(\vec{n},\vec{h})$ of the Markov chain, where $\vec{l} := \{l_i\}_{i \in \mathcal{D}}$, $\vec{k} := \{k_i\}_{i \in \mathcal{D}}$, $\vec{n} := \{n_i\}_{i \in \mathcal{D}}$ and $\vec{h} := \{h_i\}_{i \in \mathcal{D}}$. Note that $l_i, n_i \in \{1, \ldots, L\}$, and $k_i, h_i \in \{0, \ldots, K\}$. We can first decompose $p^{(\vec{n},\vec{h})}_{(\vec{l},\vec{k})}$ into two components as

$$\begin{aligned} p^{(\vec{n},\vec{h})}_{(\vec{l},\vec{k})} =& \Pr.\{\vec{Q}_{t+1} = \vec{h} | \vec{H}_t = \vec{l}, \vec{Q}_t = \vec{k}\} \times \\ & \Pr.\{\vec{H}_{t+1} = \vec{n} | \vec{H}_t = \vec{l}, \vec{Q}_t = \vec{k}, \vec{Q}_{t+1} = \vec{h}\} \\ =& p^{\vec{h}}_{(\vec{l},\vec{k})} p^{\vec{n}}_{(\vec{l},\vec{k},\vec{h})}, \end{aligned} \tag{3}$$

where the first component $p^{\vec{h}}_{(\vec{l},\vec{k})}$ is the transition probability of the queue state from $\vec{Q}_t = \vec{k}$ to $\vec{Q}_{t+1} = \vec{h}$, given the channel state $\vec{H}_t = \vec{l}$; and the second component $p^{\vec{n}}_{(\vec{l},\vec{k},\vec{h})}$ is the transition probability of the channel state from $\vec{H}_t = \vec{l}$ to $\vec{H}_{t+1} = \vec{n}$, given the queue states $\vec{Q}_t = \vec{k}$ and $\vec{Q}_{t+1} = \vec{h}$.

In the rest of Section III, we will first discuss the computation method of $p^{\vec{h}}_{(\vec{l},\vec{k})}$ and $p^{\vec{n}}_{(\vec{l},\vec{k},\vec{h})}$, respectively, to get the state transition probability $p^{(\vec{n},\vec{h})}_{(\vec{l},\vec{k})}$ of the Markov chain of $\{(\vec{H}_t, \vec{Q}_t), t = 0, 1, ...\}$ according to (3). The framework of computing $p^{(\vec{n},\vec{h})}_{(\vec{l},\vec{k})}$ in the following part is illustrated in Fig.2. Then, we will derive the steady-state distribution of the Markov chain from its state transition probability matrix and prove that the steady-state distribution exists and is unique under certain conditions in Theorem 3.

A. Transition Probability of the Queue State $p^{\vec{h}}_{(\vec{l},\vec{k})}$

According to (1) and given $r_{i,t} = R_{l_i}$, we have

$$\begin{aligned} p^{h_i}_{l_i,k_i} &= \Pr.\{Q_{i,t+1} = h_i | H_{i,t} = l_i, Q_{i,t} = k_i\} \\ &= \begin{cases} \Pr.(A_{i,t} = h_i - k_i + \eta_i) & \text{if } k_i > \eta_i, h_i \neq K \\ \Pr.(A_{i,t} = h_i) & \text{if } k_i \leq \eta_i, h_i \neq K \\ \Pr.(A_{i,t} \geq K - k_i + \eta_i) & \text{if } k_i > \eta_i, h_i = K \\ \Pr.(A_{i,t} \geq K) & \text{if } k_i \leq \eta_i, h_i = K \end{cases} \end{aligned} \tag{4}$$

where $\eta_i = \lfloor \frac{R_{l_i}\Delta T}{B} \rfloor$, and $\Pr.(A_{i,t}=a) = \frac{(\lambda_i \Delta T)^a}{a!} e^{-\lambda_i \Delta T}$ due to Poisson assumptions.

Since the transition probability $p_{l_i,k_i}^{h_i}$ of each link i depends only on its own server and queue states, we have

$$p_{(\vec{l},\vec{k})}^{\vec{h}} = \prod_{i=1}^{D} p_{l_i,k_i}^{h_i}. \tag{5}$$

B. Transition Probability of the Server State $p_{(\vec{l},\vec{k},\vec{h})}^{\vec{n}}$

According to eq.(2), the value of $SINR_{i,t}$ is determined by the (virtual) SNR vector $\vec{\gamma}_{i,t} := \{\gamma_{ji,t}\}_{j\in\mathcal{D}}$ and the queue status vector $\{\Theta_{j,t}\}_{j\in\mathcal{D}\setminus\{i\}}$. Therefore, we have the following theorem.

Definition 1: Denote the set of all possible values of Q_i as $\mathcal{S}_{Q_i}$, the set of all possible values of $\vec{Q}$ as $\mathcal{S}_Q := \prod_{i=1}^{D} \mathcal{S}_{Q_i}$, which is the Cartesian product of $\mathcal{S}_{Q_i}$, $i \in \mathcal{D}$, and the set of all possible values of $\{Q_j\}_{j\in\mathcal{D}\setminus\{i\}}$ as $\mathcal{S}_Q^{\bar{i}} := \prod_{j\in\mathcal{D}\setminus\{i\}} \mathcal{S}_{Q_j}$. Partition $\mathcal{S}_Q^{\bar{i}}$ into 2^{D-1} non-overlapping regions $\mathcal{S}_{\theta_v}^{\bar{i}}$, $v = 1,\ldots,2^{D-1}$, such that the subset of queues with non-zero queue length is identical within each region, i.e., if $\{Q_j\}_{j\in\mathcal{D}\setminus\{i\}} \in \mathcal{S}_{\theta_v}^{\bar{i}}$, then $\{\Theta_j\}_{j\in\mathcal{D}\setminus\{i\}} = \theta_v$.

Theorem 1: $\forall \vec{Q}_t = \vec{k} \in \mathcal{S}_{Q_i} \times \mathcal{S}_{\theta_v}^{\bar{i}}$ and $\forall \vec{Q}_{t+1} = \vec{h} \in \mathcal{S}_{Q_i} \times \mathcal{S}_{\theta_w}^{\bar{i}}$, the values of $p_{(l_i,\vec{k},\vec{h})}^{n_i}$ are the same and can be denoted as $p_{(l_i,\theta_v,\theta_w)}^{n_i}$.

The proof of Theorem 1 is straightforward from (2). Therefore, we try to derive the value of $p_{(l_i,\theta_v,\theta_w)}^{n_i}$, which equals

$$p_{(l_i,\theta_v,\theta_w)}^{n_i} = \frac{p_{(\theta_v,\theta_w)}^{(l_i,n_i)}}{p_{\theta_v}^{l_i}} \tag{6}$$

where

$$p_{(\theta_v,\theta_w)}^{(l_i,n_i)} = \Pr.\{H_{i,t}=l_i, H_{i,t+1}=n_i | \{\Theta_{j,t}\}_{j\in\mathcal{D}\setminus\{i\}} = \theta_v, \{\Theta_{j,t+1}\}_{j\in\mathcal{D}\setminus\{i\}} = \theta_w\} \tag{7}$$

$$p_{\theta_v}^{l_i} = \Pr.\{H_{i,t}=l_i | \{\Theta_{j,t}\}_{j\in\mathcal{D}\setminus\{i\}} = \theta_v\} \tag{8}$$

1) Derivation of $p_{\theta_v}^{l_i}$: Since $H_{i,t} = l_i$, we have $SINR_{i,t} \in [\chi_{(l_i-1)}, \chi_{l_i})$. Therefore, according to (2), $\vec{\gamma}_{i,t}$ at time slot t belongs to the convex polyhedron $\Upsilon_{l_i} := \{\vec{\gamma}_i | \gamma_{ii} - \chi_{(l_i-1)} \sum_{j\in\mathcal{D}\setminus\{i\}} \gamma_{ji}\Theta_{j,t} \geq \chi_{(l_i-1)}, \gamma_{ii} - \chi_{l_i} \sum_{j\in\mathcal{D}\setminus\{i\}} \gamma_{ji}\Theta_{j,t} < \chi_{l_i}, \vec{\gamma}_i \geq 0\}$. The (virtual) SNR regions corresponding to the channel state l_i and l_i+1 are separated by the hyperplane $\gamma_{ii} - \chi_{l_i} \sum_{j=1,j\neq i}^{D} \gamma_{ji}\Theta_{j,t} = \chi_{l_i}$. Assume there are two links in the system, an illustration of the SINR regions and its equivalent (virtual) SNR vector regions of link 1 when the channel state $H_{1,t} = 1,2,3$ and $\{\Theta_{2,t}\} = \{1\}$ is shown in Fig.3. Therefore, the steady-state probability that $H_{i,t} = l_i$ given that $\{\Theta_{j,t}\}_{j\in\mathcal{D}\setminus\{i\}} = \theta_v$ can be derived as

$$p_{\theta_v}^{l_i} = \int_{\Upsilon_{l_i}} f(\vec{\gamma}_i)\mathrm{d}\vec{\gamma}_i = \int_{\Upsilon_{l_i}} \prod_{j\in\mathcal{D}} (f(\gamma_{ji})\mathrm{d}\gamma_{ji}). \tag{9}$$

where $f(\vec{\gamma}_i)$ is the joint probability distribution function (pdf) of the stationary random process $\{\gamma_{ji,t}\}_{j\in\mathcal{D}}$, and $f(\gamma_{ji})$ is the pdf of $\gamma_{ji,t}$. The second equality is due to the independence between the r.v. elements in the set $\{\gamma_{ji}\}_{j\in\mathcal{D}}$. For a Rayleigh fading channel with additive white Gaussian noise, the received instantaneous SNR, γ_{ji}, is exponentially distributed with mean $\bar{\gamma}_{ji}$.

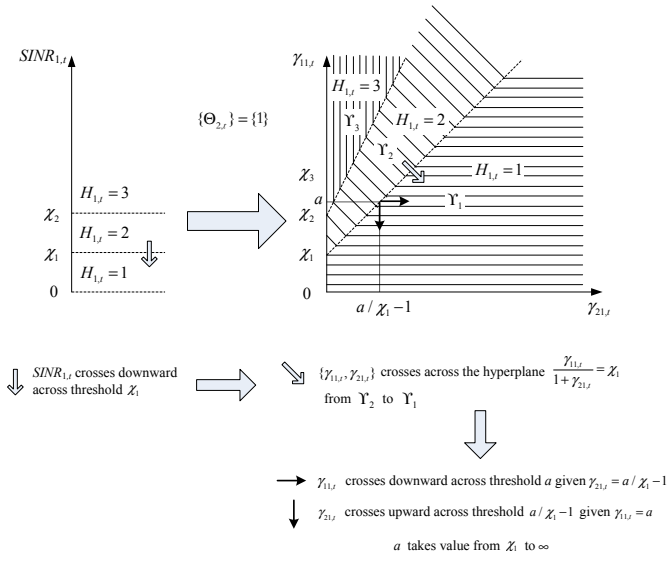

Fig. 3. (Virtual) SNR regions corresponding to the channel states and possible transitions of H_i from l_i into n_i when $v = w$.

Therefore, $p_{\theta_v}^{l_i}$ can be derived by the integration of a multivariate exponential function over a convex polyhedron, which can be equivalently written as

$$p_{\theta_v}^{l_i} = \int \cdots \int_0^{\infty} \Big(\int_{lb(l_i,\mathcal{J}_t)}^{ub(l_i,\mathcal{J}_t)} f(\gamma_{ii})\mathrm{d}\gamma_{ii} \Big) \prod_{j\in\mathcal{J}_t} f(\gamma_{ji})\mathrm{d}\gamma_{ji}, \tag{10}$$

where $ub(l_i,\mathcal{J}_t) = \chi_{l_i} + \chi_{l_i} \sum_{j\in\mathcal{J}_t} \gamma_{ji}$, $lb(l_i,\mathcal{J}_t) = \chi_{l_i-1} + \chi_{l_i-1} \sum_{j\in\mathcal{J}_t} \gamma_{ji}$. Therefore, the integration limits of γ_{ii} can be written as affine functions of $\gamma_{ji}, j \in \mathcal{J}_t$, while the integration limits of $\gamma_{ji}, j \in \mathcal{J}_t$ are all from 0 to ∞. Therefore, the closed-form expression for $p_{\theta_v}^{l_i}$ can be written as

$$p_{\theta_v}^{l_i} = \prod_{j\in\mathcal{J}_t} \frac{1}{\bar{\gamma}_{ji}} \Big(\frac{\exp(-\chi_{(l_i-1)}/\bar{\gamma}_{ii})}{\prod_{k\in\mathcal{J}_t} (1/\bar{\gamma}_{ki} + \chi_{(l_i-1)}/\bar{\gamma}_{ii})} - \frac{\exp(-\chi_{l_i}/\bar{\gamma}_{ii})}{\prod_{k\in\mathcal{J}_t} (1/\bar{\gamma}_{ki} + \chi_{l_i}/\bar{\gamma}_{ii})} \Big). \tag{11}$$

2) Derivation of $p_{(\theta_v,\theta_w)}^{(l_i,n_i)}$: The transition of channel state H_i from l_i to n_i can be due to two categories of factors: (1) the fading of link i and its potential interfering links; (2) the variation of the set of interfering links of link i from θ_v to θ_w due to the changing backlog status of the other links. Therefore, we consider that $v = w$ and $v \neq w$, respectively, and derive the value of $p_{(\theta_v,\theta_w)}^{(l_i,n_i)}$ under each scenario. In the former scenario, factor (2) doesn't exist and we can focus on the SINR variation due to the fading effects.

a) When $v = w$: the values of $\{\Theta_{j,t}\}_{j\in\mathcal{D}\setminus\{i\}}$ and $\{\Theta_{j,t+1}\}_{j\in\mathcal{D}\setminus\{i\}}$ remain the same during two consecutive time slots, and thus the set of interference links $\{I_{ji}\}_{j\in\mathcal{J}_t}$ and

$\{I_{ji}\}_{j\in\mathcal{J}_{t+1}}$ remain the same in time slot t and $t+1$. Therefore, the transition of $H_{i,t}$ in state l_i to $H_{i,t+1}$ in state n_i can only be due to the variations of the (virtual) SNR vector $\{\gamma_{ji}\}_{j\in\{i\}\bigcup\mathcal{J}_t}$ in time slot t and $t+1$. In [19], in order to derive the transition probability of the FSMC based on SNR partition, the product of the SNR level crossing rate and the time slot interval is used to approximate the joint probability that the channel states are in adjacent states in time slot t and $t+1$, respectively. Furthermore, it assumes that the joint probabilities that the channel states are in different and non-adjacent states in two consecutive time slots are zero. In this paper, we use a similar method to approximate the transition probabilities of the FSMC based on SINR partition. However, since the state transition of the SINR-based FSMC can be due to the variations of any of the (virtual) SNR elements in the (virtual) SNR vector $\{\gamma_{ji}\}_{j\in\{i\}\bigcup\mathcal{J}_t}$, the derivation method is much more complicated. We first use a similar assumption as in the SNR-based FSMC that the state transition of $H_{i,t}$ can only occur between adjacent states, i.e., $p^{(l_i,n_i)}_{(\theta_v,\theta_w)}=0$, if $|n_i-l_i|>1$. Then, we try to derive the transition probabilities between adjacent states as

$$\begin{aligned} p^{(l_i,l_i+1)}_{(\theta_v,\theta_w)} &\approx NI(\chi_{l_i})\Delta T, \\ p^{(l_i,l_i-1)}_{(\theta_v,\theta_w)} &\approx NI(\chi_{(l_i-1)})\Delta T, \end{aligned} \tag{12}$$

where $NI(\chi_{l_i})$ is "level crossing rate" in terms of the SINR, i.e., the expected number of times per second the SINR passes downward across the threshold χ_{l_i}. This approximation is similar to the method in [19]. $NI(\chi_{l_i})\Delta T$, whose value is smaller than one, can be explained as the probability that the SINR passes downward across the threshold χ_{l_i} in a time slot interval ΔT.

In order to derive the value of $NI(\chi_{l_i})\Delta T$, we consider a small time interval $\Delta t\to 0$. Therefore, $NI(\chi_{l_i})\Delta t$ can be explained as the probability that the SINR passes downward across the threshold χ_{l_i} in a small interval Δt.

Theorem 2: We find the SINR value of link i crosses downward the threshold χ_{l_i} in a small time interval Δt if one of the mutually exclusive and exhaustive eventualities in the set $\{E_j\}_{j\in\{i\}\bigcup\mathcal{J}_t}$ occurred, where E_j is defined as the event that the (virtual) SNR γ_{ji} passes downward (or upward) across a threshold Γ_{j,l_i}, which equals

$$\Gamma_{j,l_i}=\begin{cases} \frac{1}{\chi_{l_i}}(\gamma_{ii}-\chi_{l_i}(1+\sum_{k\in\mathcal{D}\setminus\{i,j\}}\gamma_{ki}\Theta_{j,t})), & \text{if } j\neq i, \\ \chi_{l_i}(1+\sum_{k\in\mathcal{D}\setminus\{i\}}\gamma_{ki}\Theta_{j,t}), & \text{if } j=i, \end{cases} \tag{13}$$

while the other (virtual) SNR values in the set $\{\gamma_{ki}\}_{k\in\{i\}\bigcup\mathcal{J}_t}$ remain unchanged. The probability of event E_j can be calculated as

$$\Pr.(E_j)=\int\cdots\int N_j(\Gamma_{j,l_i})\Delta t\prod_{k\in\{i\}\bigcup\mathcal{J}_t\setminus\{j\}}f(\gamma_{ki})\mathrm{d}\gamma_{ki}, \tag{14}$$

where $N_j(\Gamma), j=1,\ldots,D$ is the level crossing rate of the (virtual) SNR γ_{ji} at Γ, which is the expected number of times per second the (virtual) SNR γ_{ji} passes downward (or upward) across the threshold Γ, and can be calculated according to the Doppler shift f_m and the normalized threshold $\Gamma/\bar{\gamma}_{ji}$ [19].

Proof: Due to the equivalence between the SINR region $[\chi_{(l_i-1)},\chi_{l_i})$ and the (virtual) SNR region Υ_{l_i} when the channel state $H_{i,t}=l_i,(l_i=1,\ldots,L)$, the SINR value of link i crosses downward the threshold χ_{l_i} if and only if the (virtual) SNR vector $\vec{\gamma}_i$ passes across the hyperplane $\gamma_{ii}-\chi_{l_i}\sum_{j\in\mathcal{D}\setminus\{i\}}\gamma_{ji}\Theta_{j,t}=\chi_{l_i}$ from the convex polyhedron Υ_{l_i+1} to Υ_{l_i} in a small interval Δt. Consider a (virtual) SNR γ_{ji} for $j\in\{i\}\bigcup\mathcal{J}_t$, given the values of the rest of the (virtual) SNR elements in the set $\{\gamma_{ki}\}_{k\in\{i\}\bigcup\mathcal{J}_t}$, we can derive the (virtual) SNR threshold Γ_{j,l_i} according to (13) so that if γ_{ji} crosses downward (or upward) Γ_{j,l_i} then the (virtual) SNR vector $\vec{\gamma}_i$ crosses the hyperplane $\gamma_{ii}-\chi_{l_i}\sum_{j=1,j\neq i}^{D}\gamma_{ji}\Theta_{j,t}=\chi_{l_i}$ from the convex polyhedron Υ_{l_i+1} to Υ_{l_i}. Since $N_j(\Gamma)\Delta t$ is the probability that the (virtual) SNR γ_{ji} passes downward (or upward) across the threshold Γ in a small interval Δt, and the values of the rest of the (virtual) SNR elements in the set $\{\gamma_{ki}\}_{k\in\{i\}\bigcup\mathcal{J}_t}$ can be taken over the field of non-negative real numbers as long as $\Gamma_{j,l_i}>0$ with the pdf function $f(\gamma_{ki})$, the probability of event E_j can be derived as (14).

Note that the probability of multiple simultaneous variations of the (virtual) SNR elements in the vector $\vec{\gamma}_i$ in a small interval Δt are prohibited in the sense that each such multiple event is of order $\mathrm{o}(\Delta t)$. Therefore, we will find the SINR value of link i crosses downward the threshold χ_{l_i}, or equivalently the (virtual) SNR vector $\vec{\gamma}_i$ crosses the hyperplane $\gamma_{ii}-\chi_{l_i}\sum_{j\in\mathcal{D}\setminus\{i\}}\gamma_{ji}\Theta_{j,t}=\chi_{l_i}$ from the convex polyhedron Υ_{l_i+1} to Υ_{l_i} in a time interval Δt, if one of the mutually exclusive and exhaustive eventualities $E_j,\ j\in\{i\}\bigcup\mathcal{J}_t$ occurred. ■

Example 1: As illustrated in Fig.3 where there are two links and three channel states of $H_{i,t},\ i=1,2$, we consider the link 1 and assume that $\{\Theta_{2,t}\}=\{\Theta_{2,t+1}\}=\theta_v=\{1\}$, i.e., link 1 suffers interference from link 2 in both time slots t and $t+1$. $SINR_{i,t}$ crosses downward across threshold χ_1 so that $H_{1,t}=2$ and $H_{1,t+1}=1$. This is equivalent to $\{\gamma_{11,t},\gamma_{21,t}\}$ crosses across the hyperplane $\frac{\gamma_{11,t}}{1+\gamma_{21,t}}=\chi_1$ from Υ_2 to Υ_1, which can only happen when $\gamma_{11,t}$ crosses downward across threshold a while $\gamma_{21,t}=a/\chi_1-1$ remains unchanged or $\gamma_{21,t}$ crosses upward across threshold $\gamma_{21,t}=a/\chi_1-1$ while $\gamma_{11,t}=a$ remains unchanged, where a takes values over the region $[\chi_1,\infty)$.

According to Theorem 2, we have

$$NI(\chi_{l_i})\Delta t=\sum_{j\in\mathcal{D}}\Pr.(E_j). \tag{15}$$

Let both sides of (15) be divided by Δt, we can derive the level crossing rate $NI(\chi_{l_i})$ of the SINR value of link i. Combining (15) with (12), we have

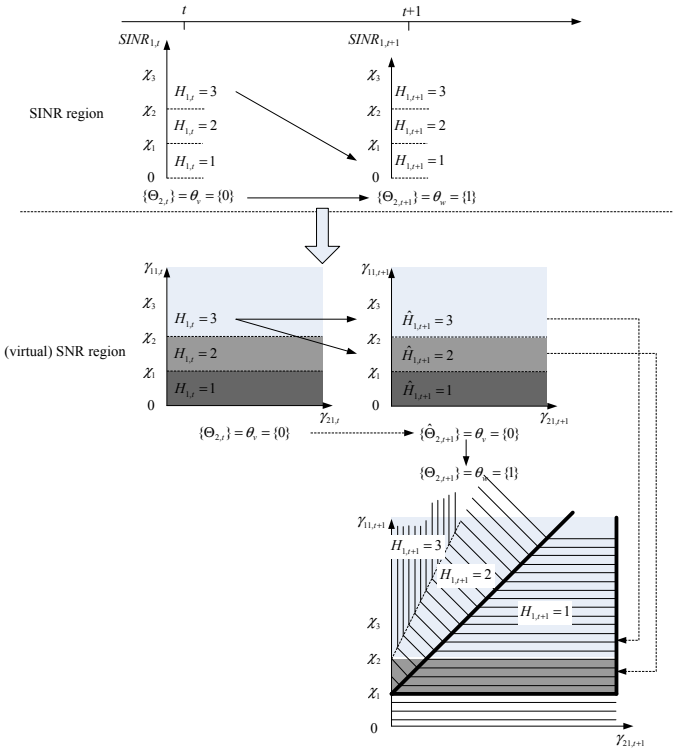

Fig. 4. Possible transitions of H_i from l_i into n_i when $v \neq w$.

$$p_{(\theta_v,\theta_v)}^{(l_i,l_i+1)} \approx \sum_{j=1}^{D} \int \cdots \int_0^{\infty} N_j(\Gamma_{j,l_i})\Delta T \prod_{k\in\{i\}\bigcup\mathcal{J}_t\setminus\{j\}} f(\gamma_{ki})\mathrm{d}\gamma_{ki},$$
$$p_{(\theta_v,\theta_v)}^{(l_i,l_i-1)} \approx \sum_{j=1}^{D} \int \cdots \int_0^{\infty} N_j(\Gamma_{j,(l_i-1)})\Delta T \prod_{k\in\{i\}\bigcup\mathcal{J}_t\setminus\{j\}} f(\gamma_{ki})\mathrm{d}\gamma_{ki}. \quad (16)$$

b) When $v \neq w$: the values of $\{\Theta_{j,t}\}_{j\in\mathcal{D}\setminus\{i\}}$ and $\{\Theta_{j,t+1}\}_{j\in\mathcal{D}\setminus\{i\}}$ are different during two consecutive time slots. Therefore, the transition of $H_{i,t}$ from state l_i to $H_{i,t+1}$ in state n_i can be due to not only the variations of the (virtual) SNR vector $\{\gamma_{ji}\}_{j\in\{i\}\bigcup\mathcal{J}_t}$ in time slot t and $t+1$, but also the change of interference link set from $\{I_{ji}\}_{j\in\mathcal{J}_t}$ to $\{I_{ji}\}_{j\in\mathcal{J}_{t+1}}$. Therefore, we can no longer assume that the state transition of $H_{i,t}$ can only occur between adjacent states. Given θ_v and θ_w, we find the channel state $H_{i,t}$ in l_i and $H_{i,t+1}$ in n_i, respectively, if one of the three following (mutually exclusive and exhaustive) eventualities occurred:

1) that due to (virtual) SNR variations from $\bar{\gamma}_{i,t}$ to $\bar{\gamma}_{i,t+1}$, we would have found the channel state $H_{i,t}$ in state l_i and $\hat{H}_{i,t+1}$ in state l_i+1 at the beginning of time slot t and $t+1$, respectively, if the value of $\{\hat{\Theta}_{j,t+1}\}_{j\in\mathcal{D}\setminus\{i\}}$ remains unchanged as $\{\Theta_{j,t}\}_{j\in\mathcal{D}\setminus\{i\}}$, which equals θ_v; however, since $\{\Theta_{j,t+1}\}_{j\in\mathcal{D}\setminus\{i\}}$ changes to θ_w at the beginning of time slot $t+1$, $H_{i,t+1}$ is in state n_i instead of state l_i+1 with the same set of underlying (virtual) SNR vector values $\bar{\gamma}_{i,t+1}$; the multi-transition path described above is denoted as $H_{i,t} = l_i \rightarrow \hat{H}_{i,t+1} = l_i+1 \rightarrow H_{i,t+1} = n_i$;
2) that similar to event 1), except that $\hat{H}_{i,t+1} = l_i - 1$, i.e., $H_i(t) = l_i \rightarrow \hat{H}_{i,t+1} = l_i - 1 \rightarrow H_{i,t+1} = n_i$;
3) that similar to event 1), except that $\hat{H}_{i,t+1} = l_i$, i.e., $H_i(t) = l_i \rightarrow \hat{H}_{i,t+1} = l_i \rightarrow H_{i,t+1} = n_i$.

Example 2: As illustrated in Fig.4 where there are two links and three channel states of $H_{i,t},\ i = 1, 2$, we consider the link 1 and assume that $\{\Theta_{2,t}\} = \theta_v = \{0\}$ and $\{\Theta_{2,t+1}\} = \theta_w = \{1\}$, i.e., link 1 suffers no interference from link 2 in time slot t, but it receives interference in time slot $t+1$. We consider that $H_{1,t}$ is in state 3 and $H_{1,t+1}$ is in state 1 as shown in the upper part of Fig.(4) and examine the events that can cause this to happen as shown in the lower part of Fig.(4), which maps the SINR regions corresponding to the three states of $H_{1,t}$ to the (virtual) SNR regions. The solid lines mean that there is a change in the (virtual) SNR or the queue status, while the dotted lines mean no change has happened. First, assume that $\{\hat{\Theta}_{2,t+1}\}$ is unchanged as $\{\Theta_{2,t}\} = \{0\}$, and $\hat{H}_1(t+1)$ can transit to the adjacent state 2 or remain in the same state 3 as $H_1(t)$. The (virtual) SNR region $\vec{\gamma}_{1,t+1}$ corresponding to both states are shown in Fig.(4) as light gray and medium gray areas. Second, since $\{\Theta_{2,t+1}\}$ is $\{1\}$ instead of $\{0\}$, $H_{1,t+1}$ is in state 1 instead of state 2 or state 3, and its corresponding (virtual) SNR region $\vec{\gamma}_{1,t+1}$ falls in the region surrounded by the bold lines, i.e., the overlapping regions of the horizontal stripped area with the light gray and medium gray areas. The multi-transition paths of the above two events are $H_{1,t} = 3 \rightarrow \hat{H}_{1,t+1} = 3 \rightarrow H_{1,t+1} = 1$ and $H_{1,t} = 3 \rightarrow \hat{H}_{1,t+1} = 2 \rightarrow H_{1,t+1} = 1$.

Therefore, we have

$$p_{(\theta_v,\theta_w)}^{(l_i,n_i)} = p_{(\theta_v,\theta_v)}^{(l_i,l_i+1)} \times \hat{p}_{(l_i+1,\theta_v,\theta_w)}^{n_i} + p_{(\theta_v,\theta_v)}^{(l_i,l_i-1)} \times \hat{p}_{(l_i-1,\theta_v,\theta_w)}^{n_i} + p_{(\theta_v,\theta_v)}^{(l_i,l_i)} \times \hat{p}_{(l_i,\theta_v,\theta_w)}^{n_i}, \quad (17)$$

where $p_{(\theta_v,\theta_v)}^{(l_i,l_i)}$ (resp. $p_{(\theta_v,\theta_v)}^{(l_i,l_i+1)}$, $p_{(\theta_v,\theta_v)}^{(l_i,l_i-1)}$) is the conditional joint probability that $H_{i,t}$ is in state l_i and $\hat{H}_{i,t+1}$ is in state l_i (resp. l_i+1, l_i-1), given that $\{\hat{\Theta}_{j,t+1}\}_{j\in\mathcal{D}\setminus\{i\}} = \{\Theta_{j,t}\}_{j\in\mathcal{D}\setminus\{i\}} = \theta_v$, whose value can be derived from (16). On the other hand, $\hat{p}_{(l_i,\theta_v,\theta_w)}^{n_i}$ (resp. $\hat{p}_{(l_i+1,\theta_v,\theta_w)}^{n_i}$, $\hat{p}_{(l_i-1,\theta_v,\theta_w)}^{n_i}$) represents the conditional probability that $\hat{H}_{i,t+1}$ is in state n_i, given that $\{\hat{\Theta}_{j,t+1}\}_{j\in\mathcal{D}\setminus\{i\}} = \theta_v$, $\hat{H}_{i,t+1}$ is in state l_i (resp. l_i+1, l_i-1), and $\{\Theta_{j,t+1}\}_{j\in\mathcal{D}\setminus\{i\}} = \theta_w$, i.e.,

$$\hat{p}_{(l_i,\theta_v,\theta_w)}^{n_i} = \Pr.\{H_i(t+1) = n_i | \hat{H}_i(t+1) = l_i, \{\hat{\Theta}_{j,t+1}\}_{j\in\mathcal{D}\setminus\{i\}} = \theta_v, \{\Theta_{j,t+1}\}_{j\in\mathcal{D}\setminus\{i\}} = \theta_w\}. \quad (18)$$

Given that $\hat{H}_i(t+1) = l_i$ and $\{\hat{\Theta}_{j,t+1}\}_{j\in\mathcal{D}\setminus\{i\}} = \theta_v$, the (virtual) SNR vector $\vec{\gamma}_{i,t+1}$ belongs to the convex polyhedron $\Upsilon_{l_i} := [\vec{\gamma}_i | \gamma_{ii} - \chi_{(l_i-1)} \sum_{j\in\mathcal{D}\setminus\{i\}} \gamma_{ji}\hat{\Theta}_{j,t+1} \geq \chi_{(l_i-1)}, \gamma_{ii} - \chi_{l_i} \sum_{j\in\mathcal{D}\setminus\{i\}} \gamma_{ji}\hat{\Theta}_{j,t+1} < \chi_{l_i}, \vec{\gamma}_i \geq 0\}$. Similarly, given $H_i(t+1) = n_i$ and $\{\Theta_{j,t+1}\}_{j\in\mathcal{D}\setminus\{i\}} = \theta_w$, $\vec{\gamma}_{i,t+1}$ also belongs to the convex polyhedron $\Upsilon_{n_i} := \{\vec{\gamma}_i | \gamma_{ii} - \chi_{(n_i-1)} \sum_{j\in\mathcal{D}\setminus\{i\}} \gamma_{ji}\Theta_{j,t+1} \geq \chi_{(n_i-1)}, \gamma_{ii} - \chi_{n_i} \sum_{j\in\mathcal{D}\setminus\{i\}} \gamma_{ji}\Theta_{j,t+1} < \chi_{n_i}, \vec{\gamma}_i \geq 0\}$. Therefore, the

(virtual) SNR vector $\vec{\gamma}_{i,t+1}$ should belong to the convex polyhedron $\Upsilon_{l_i} \bigcap \Upsilon_{n_i}$, and

$$\hat{p}^{n_i}_{(l_i,\theta_v,\theta_w)} = \frac{\hat{p}^{l_i,n_i}_{(\theta_v,\theta_w)}}{p^{l_i+1}_{\theta_v}}, \tag{19}$$

where

$$\begin{aligned}\hat{p}^{(l_i,n_i)}_{(\theta_v,\theta_w)} =& \Pr.\{\hat{H}_i(t+1) = l_i, H_i(t+1) = n_i| \\ & \{\hat{\Theta}_{j,t+1}\}_{j\in\mathcal{D}\backslash\{i\}} = \theta_v, \{\Theta_{j,t+1}\}_{j\in\mathcal{D}\backslash\{i\}} = \theta_w\} \\ =& \int_{\Upsilon_{l_i}\bigcap\Upsilon_{n_i}} f(\vec{\gamma}_{i,t+1})\mathrm{d}\vec{\gamma}_{i,t+1},\end{aligned} \tag{20}$$

$$p^{l_i+1}_{\theta_v} = \Pr.\{\hat{H}_i(t+1) = l_i|\{\hat{\Theta}_{j,t+1}\}_{j\in\mathcal{D}\backslash\{i\}} = \theta_v\}. \tag{21}$$

The denominator of (19) can be derived according to (11). Similar to (10), the numerator of (19) is also the integration of a multivariate exponential over a convex polyhedron according to (20). However, since

$$\begin{aligned}\gamma_{ii} \in \big[& \max\{lb(l_i,\mathcal{J}_{i,t}), lb(n_i,\mathcal{J}_{i,t+1})\}, \\ & \min\{ub(l_i,\mathcal{J}_{i,t}), ub(n_i,\mathcal{J}_{i,t+1})\}\big],\end{aligned} \tag{22}$$

the integration limits of γ_{ii} cannot be written as affine functions of $\gamma_{ji}, j \in \mathcal{D}\backslash\{i\}$. Since integration over an arbitrary convex polyhedron is a non-trivial problem, and it has been shown that computing the volume of polytopes of varying dimension is NP-hard, we present a relatively simple method to calculate the integration of (20) in the appendix A.

Similar to (19), we can derive the values of $p^{n_i}_{(l_i+1,\theta_v,\theta_w)}$ and $p^{n_i}_{(l_i-1,\theta_v,\theta_w)}$. Taking these values into (17), we can derive the value of $p^{(l_i,n_i)}_{(\theta_v,\theta_w)}$ when $v \neq w$.

Now we have derived both the values of the denominator (by (11)) and numerator (by (16) when $v = w$ and by (17) when $v \neq w$) in (6), we can finalize the calculation of $p^{n_i}_{(l_i,\theta_v,\theta_w)}$ and thus $p^{n_i}_{(l_i,\vec{k},\vec{h})}$.

Finally, we have

$$p^{\vec{n}}_{(\vec{l},\vec{k},\vec{h})} = \prod_{i=1}^{D} p^{n_i}_{(l_i,\vec{k},\vec{h})}. \tag{23}$$

C. Steady-State Probability of Markov chain $\{\vec{H}_t, \vec{Q}_t\}$

Define the transition probability matrix $\mathbf{P} = [p^{(\vec{n},\vec{h})}_{(\vec{l},\vec{k})}]$ and the steady-state probability matrix $\boldsymbol{\pi} = [\pi_{\vec{l},\vec{k}}]$, where $\pi_{\vec{l},\vec{k}} \equiv \lim_{t\to\infty} \Pr.\{\vec{H}_t = \vec{l}, \vec{Q}_t = \vec{k}\}$. Each element of the transition probability matrix $\mathbf{P}$ can be derived from (3) combining with (5) and (23).

Theorem 3: The stationary distribution of the Markov chain $(\vec{H}_t, \vec{Q}_t)$ exists; $\boldsymbol{\pi}$ is unique, and $\boldsymbol{\pi} > 0$.

Theorem 3 is proved in Appendix B. Then, the stationary distribution of the ergodic process $\{\vec{H}_t, \vec{Q}_t\}$ can be uniquely determined from the balance equations

$$\boldsymbol{\pi} = \boldsymbol{\pi}\mathbf{P}, \ \boldsymbol{\pi}\mathbf{e} = 1. \tag{24}$$

where $\mathbf{e}$ is the unity vector of dimension $(L \times (K+1))^D$ and $\boldsymbol{\pi}$ can be derived as the normalized left eigenvector of $\mathbf{P}$ corresponding to eigenvalue 1.

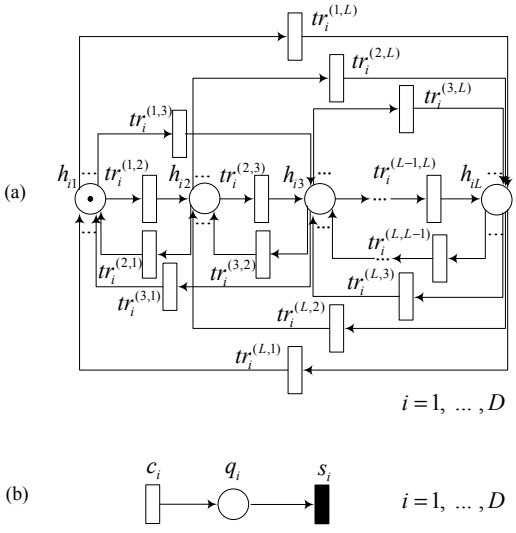

Fig. 5. The DSPN Model of FR strategy. (a) The service process in SPN, (b) The queue process in DSPN.

IV. Model Decomposition and Performance Approximation using DSPN

A. The DSPN Model

The analytical method in the previous section for the multi-user system faces the challenge of the exponentially enlarged state space, which makes it unacceptable for a large number of links. Since directly solving the queuing model suffers the high computational complexity, in this section, we formulate the SPN model of the above queuing system and use the model decomposition and an iteration procedure of SPN to simplify the analysis.

The $(2 \times D)$-dimensional discrete-time Markov chain $\{(\vec{H}_t, \vec{Q}_t), t = 0, 1, ...\}$ can be seen as a sampled-time Markov chain of a continuous-time semi-Markov process sampled at every ΔT interval, while the continuous-time semi-Markov process can be modeled as a Deterministic Stochastic Petri Nets (DSPN). The DSPN consists of a SPN for representing service processes and a DSPN for representing queuing processes. The SPN, as shown in Fig.5(a), is composed of D subnets and each subnet i corresponds to the L-state Markov modulated service process of link i. Each subnet is described by places $(\{h_{il}\}_{l=1}^{L})$ and transitions $\{tr_i^{(l,n)}\}_{l,n=1,l\neq n}^{L}$. The DSPN, as shown in Fig. 5(b), models the queuing behavior of the links and can be characterized by places $\{q_i\}_{i\in\mathcal{D}}$, and transitions $\{c_i\}_{i\in\mathcal{D}}$, $\{s_i\}_{i\in\mathcal{D}}$. The meanings of all the places and transitions are described as follows.

- h_{il}: a place for the l-th channel state of link i.
- $tr_i^{(l,n)}$: exponentially-distributed timed transitions for the channel state transitions of link i. When $tr_i^{(l,n)}$ fires, the channel state transits from l to n. The firing rate of $tr_i^{(l,n)}$ can be derived as $\rho_i^{(l,n)} = p^n_{(l,\vec{k},\vec{h})}/\Delta T$, where $p^n_{(l,\vec{k},\vec{h})}$ can be obtained by (6). Therefore, $\rho_i^{(l,n)}$ depends on the queue states of the other links before and after h_{il} transits to h_{in}, i.e., whether $M(q_j), (j \in \mathcal{D}\backslash\{i\})$, is equal to or larger

than zero, where $M(\cdot)$ is a mapping function from a place to the number of tokens assigned to it. Note that transitions from any channel state $h_{il},\ l \in \{1,\ldots,L\}$ to any other channel states $h_{in},\ n \in \{1,\ldots,L\}\backslash\{i\}$ are possible as proved in Lemma 1.

q_i: a place for the queue state of link i.

c_i: an exponentially-distributed timed transition denoting new packet arrivals from link i, with firing rate λ_i. When it fires, one packet arrives at the queue place q_i.

s_i: a deterministic timed transitions for service process. When it fires, one packet is transmitted from the queue place q_i. Its firing rate μ_i depends on the marking of the places $\{h_{il}\}_{l=1}^{L}$, i.e.,

$$\mu_i = \lfloor \frac{R_l \Delta T}{B} \rfloor / \Delta T, \text{ if } M(h_{il}) = 1,\ l = 1,\ldots,L, \tag{25}$$

where $M(h_{il})$ is either 1 or 0, which represents whether link i is in its l-th channel state or not.

B. Model Decomposition and Iteration

According to [22], the original DSPN can be decomposed into a set of "near-independent" subnets. By decomposition, the original multiuser system is represented by D subsystems, each of which consists of one subnet in Fig. 5(a) and one subnet in Fig. 5(b). Obviously, if each subsystem can be analyzed separately, the model decomposition can significantly reduce the size of the state space in the analysis and achieves better performance in computational complexity. However, unfortunately, such model decomposition is not 'clean', i.e., there exist interactions among subsystems. Specifically, for any subsystem $i \in \mathcal{D}$, the firing rate of transition s_i depends on the marking of the places $\{h_{il}\}_{l=1}^{L}$, which in turn depends on the markings of the queue places q_j of those links $j \in \mathcal{D}\backslash\{i\}$. As a consequence, the markings of all other subsystems have to be available at the same time in order to solve the i-th subsystem, which is not possible in the decomposed model. In order to solve this dilemma, we use the fixed point iteration method in Stochastic Petri Nets [23]. First, the steady-state probabilities of the markings instead of the instant markings of the other subsystems are used as the input of subsystem i in order to derive its steady-state probabilities of the markings. Next, fixed point iteration is used to deal with the cycles in the model solution process.

Let $\{H_{i,t}, Q_{i,t}\}$ denote the the sampled-time Markov chain for the i-th DSPN subsystem. Let $\boldsymbol{\pi}_i := [\pi^i_{l_i,k_i}]$ denote the steady-state probabilities of $\{H_{i,t}, Q_{i,t}\}$, where $\pi^i_{l_i,k_i} \equiv \lim_{t\to\infty} \Pr.\{H_{i,t} = l_i, Q_{i,t} = k_i\}$. In order to derive the steady-state probabilities $\boldsymbol{\pi}_i$ of subsystem i, we have to first derive the transition probability matrix $\mathbf{P}_i = [p^{(n_i,h_i)}_{(l_i,k_i)}]$. First, $p^{h_i}_{(l_i,k_i)}$ can be derived according to (4). Next, we try to analyze the transition probability of the channel state from l_i to n_i given the queue states (k_i, h_i). According to (6), we can derive the value of $p^{n_i}_{(l_i,\vec{k},\vec{h})}$. However, since only the queue state (k_i, h_i) of subsystem i is given instead of $(\vec{k}, \vec{h})$, we assume that the steady state probabilities of all the other subsystems $\{\boldsymbol{\pi}_j\}^{D}_{j\in\mathcal{D}\backslash\{i\}}$ are known and derive the approximate transition probability $\widetilde{p}^{n_i}_{(l_i,k_i,h_i)}$ as follows:

$$\widetilde{p}^{n_i}_{(l_i,k_i,h_i)} = \sum_{\substack{\{k_j\}_{j\in\mathcal{D}\backslash\{i\}}\in\mathcal{S}^{\bar{i}}_Q \\ \{h_j\}_{j\in\mathcal{D}\backslash\{i\}}\in\mathcal{S}^{\bar{i}}_Q}} p^{n_i}_{(l_i,\vec{k},\vec{h})} \prod_{j\in\mathcal{D}\backslash\{i\}} \pi_{k_j,h_j}. \tag{26}$$

where $\pi_{k_j,h_j} \equiv \lim_{t\to\infty} \Pr.\{Q_{j,t} = k_j, Q_{j,t+1} = h_j\}$ is the joint steady-state probability that the queue length of link j is k_j in time slot t and h_j in time slot $t+1$. Therefore, we have,

$$\pi_{k_j,h_j} = \sum_{l_j=1}^{L} p^{h_j}_{l_j,k_j} \pi^j_{l_j,k_j}, \tag{27}$$

where $p^{h_j}_{l_j,k_j}$ can be obtained by (4).

Finally, we have

$$\widetilde{p}^{(n_i,h_i)}_{(l_i,k_i)} = p^{h_i}_{(l_i,k_i)} \widetilde{p}^{n_i}_{(l_i,k_i,h_i)}, \tag{28}$$

which gives the transition probability matrix $\mathbf{P}_i$, and the steady state probabilities $\boldsymbol{\pi}_i$ can be derived similar to (24).

Define $\mathbf{x}_j := \{\pi_{k_j,h_j}\}^{K}_{k_j,h_j=0}$. According to (26), the solution $\boldsymbol{\pi}_i$ for the i-th subsystem can be obtained only when the measure $\{\mathbf{x}_j\}_{j\in\mathcal{D}\backslash\{i\}}$ are known so that the transition matrix $\mathbf{P}_i$ can be derived, and the value of $\{\mathbf{x}_j\}_{j\in\mathcal{D}\backslash\{i\}}$ depends on the solutions of all the other subsystems $\{\boldsymbol{\pi}_j\}_{j\in\mathcal{D}\backslash\{i\}}$ according to (27). Obviously, if the D subsystems are solved sequentially by index, the above requirement cannot be satisfied since only $\{\mathbf{x}_j\}^{i-1}_{j=1}$ are known when solving the i-th subsystem. In the following, the fixed point iteration method is used to solve this problem.

Let $\{\mathbf{x}_1,\ldots,\mathbf{x}_D\}$ be the vector of *iteration variables* of the *fixed point equation*

$$\{\mathbf{x}_1,\ldots,\mathbf{x}_D\} = z(\{\mathbf{x}_1,\ldots,\mathbf{x}_D\}), \tag{29}$$

where the function z is realized by solving the D subsystems successively with the subsystem solution method as described in the previous subsection. That is, the function z can be decomposed into D independent functions $z_i,\ i \in \mathcal{D}$, with z_i representing the derivation of the solution $\boldsymbol{\pi}_i$ from the measure $\{\mathbf{x}_1,\ldots,\mathbf{x}_D\}$, and the calculation of the measure $\mathbf{x}_i$ as a function z'_i of $\boldsymbol{\pi}_i$ according to (27), i.e.,

$$\begin{aligned} \mathbf{x}_i &= z'_i(\boldsymbol{\pi}_i(\{\mathbf{x}_1,\ldots,\mathbf{x}_D\})) \\ &= z_i(\{\mathbf{x}_1,\ldots,\mathbf{x}_D\}). \end{aligned} \tag{30}$$

Obviously, the vector of measures of the D subsystems $\{\mathbf{x}_1,\ldots,\mathbf{x}_D\}$ satisfies (29), which is referred to as the *fixed point* of this equation.

The fixed point can be derived by *successive substitution* [23]. Let the initial vector of iteration variables be $\{\mathbf{x}^0_1,\ldots,\mathbf{x}^0_D\}$. Each element of $\mathbf{x}^0_i$ $(i \in \mathcal{D})$ can be set to an arbitrary value between 0 and 1. In the u-th iteration, we have

$$\{\mathbf{x}^u_1,\ldots,\mathbf{x}^u_D\} = z(\{\boldsymbol{\pi}^{u-1}_1,\ldots,\boldsymbol{\pi}^{u-1}_D\}), \tag{31}$$

where the iteration variables are determined by the function z based on the values of the last iteration, and the

function z is realized by solving the D subsystems successively using the solution method as described above. Specifically, in solving the i-th subsystem in the u-th iteration, $\{\mathbf{x}_1^u, \ldots, \mathbf{x}_{i-1}^u, \mathbf{x}_i^{u-1}, \ldots, \mathbf{x}_D^{u-1}\}$ is used as the input to derive the value of $\mathbf{x}_i^u$. After that, $\mathbf{x}_i^{u-1}$ is replaced by $\mathbf{x}_i^u$ as input in solving the rest of the subsystems (from the $(i+1)$-th to the D-th subsystems) during the u-th iteration.

The iteration is terminated when the differences between the iteration variables of two successive iterations are less than a certain threshold value. The convergence of the fixed point iteration is proved in the Appendix C.

Given $\boldsymbol{\pi}$, the performance metrics such as the average queue length, the mean throughput, the average packet delay and the packet dropping probability can be derived as in [24].

- The average queue length of link i equals

$$\overline{Q}_i = \sum_{k_i=0}^{K} \sum_{l_i=1}^{L} \pi_{l_i,k_i}^i k_i, \tag{32}$$

  where $\sum_{l_i=1}^{L} \pi_{l_i,k_i}^i$ is the probability that $Q_{i,t} = k_i$.
- The mean throughput of link i in terms of packets/s can be expressed as

$$\overline{T}_i = \sum_{l_i=1}^{L} \sum_{k_i=1}^{K} T_{l_i,k_i} \pi_{l_i,k_i}^i, \tag{33}$$

  where

$$T_{l_i,k_i} = \begin{cases} \lfloor \frac{r_{i,t}\Delta T}{B} \rfloor / \Delta T & \text{if } k_i \geq \lfloor \frac{r_{i,t}\Delta T}{B} \rfloor \\ \frac{k_i}{\Delta T} & \text{if } k_i < \lfloor \frac{r_{i,t}\Delta T}{B} \rfloor \end{cases} \tag{34}$$

  is the service rate of link i in terms of packets/s when $H_{i,t} = l_i$ and $Q_{i,t} = k_i$. It depends on the minimum value of the channel transmission capability and the amount of packets in the queue of link i. Note that the service rate is 0 when queue i is empty ($k_i = 0$). Therefore, $\overline{T}_i$ is the sum over the whole system state space of the product between the service rate of link i in state (l_i, k_i) and the probability that the system is in state (l_i, k_i).
- The average packet delay of link i can then be calculated according to Little's Law as

$$\overline{D}_i = \overline{Q}_i / \overline{T}_i, \tag{35}$$

  which is the average amount of time between the arrival and departure of a packet for link i. Note that the mean throughput $\overline{T}_i$ equals the effective arrival rate of link i, which is the average rate at which the packets enter queue i.
- Let B_{l_i,k_i}^i be the random variable which represents the number of dropped packets of link i when $H_{i,t} = l_i$ and $Q_{i,t} = k_i$. Since $K + b = A_{i,t} + \max[0, k - \lfloor \frac{r_{i,t}\Delta T}{B} \rfloor]$, where b is the number of packets dropped during the t-th slot,

$$\Pr.(B_{l_i,k_i}^i = b) = \Pr.(A_{i,t} = K + b - \max[0, k_i - \lfloor \frac{r_{i,t}\Delta T}{B} \rfloor]). \tag{36}$$

  Then, the packet dropping probability p_{d}^i of link i can be estimated as

$$\begin{aligned} p_{\mathrm{d}}^i &= \frac{\text{Average \# of packets dropped in a time slot}}{\text{Average \# of packets arrived in a time slot}} \\ &= \frac{\sum_{l_i=1}^{L} \sum_{k_i=0}^{K} \sum_{b=0}^{\infty} b \Pr.(B_{l_i,k_i} = b) \pi_{l_i,k_i}^i}{\lambda_i \Delta T}. \end{aligned} \tag{37}$$

V. Performance Evaluation

In this section, we verify our analytical model under different interference conditions by tuning the length of the potential interfering links as shown in Fig.6. We consider the path loss channel model $28 + 40 \log_{10} d$ [32] for all the D2D links and potential interfering links, where d is the distance between the transmitter and receiver in meter. We normalize the distance between a transmitter and a receiver with mean SNR equals 0dB to be 1. The distance between a transmitter and a receiver of a link is denoted as α. Note that we do not require the length of the links to be the same in our analytical model, and this assumption in our network topology is only to facilitate us to focus on the variation of the potential interfering link length. Assume that the distances between the pair of transmitters (resp. receivers) of link i and $i+1$ are $\beta + \Delta\beta(i-1)$ $(i = 1, \ldots, D-1)$. Therefore, the length of the potential interfering link I_{ji} of link i, where $j > i$ (resp. $j < i$), is $\sqrt{\alpha^2 + \left(\sum_{k=i}^{j-1}(\beta + \Delta\beta(k-1))\right)^2}$ (resp. $\sqrt{\alpha^2 + \left(\sum_{k=j}^{i-1}(\beta + \Delta\beta(k-1))\right)^2}$). In this way, we can increase (resp. decrease) the length of all the potential interfering links of link i by increase (resp. decrease) the value of β. We add $\Delta\beta(i-1)$ to β in the distance between the transmitters of link i and $i+1$ to ensure that the mean virtual SNR values $\bar{\gamma}_{ji}$ and $\bar{\gamma}_{ki}$ of any two potential interfering links I_{ji} and I_{ki} $(k \neq j \in \mathcal{D} \backslash \{i\})$ of link i are different, as required in (39).

The FSMC model has 16 states in total, and the SINR thresholds and the corresponding transmission rates in 1.4MHz bandwidth for each service process are given in Table II as defined in the LTE system. The carrier frequency f and the time slot duration ΔT are set to 2GHz and 1ms, respectively. The velocity of the terminals is set to be 3km/h so that the Doppler frequency becomes 5.56Hz. We let the buffer size $K = 50$ packets, where the packet length $B = 50$ bits.

We numerically solve the decomposed Markov model using fixed point iteration and compare the performance measures with those obtained by discrete-event simulations of a D2D communications system with dynamic packet arrivals and full frequency reuse between D2D links. Both numeric method and simulation are implemented in Matlab and all experiments are run on 1.93GHz PC with 1.87GHz RAM. We increase the link number D from 2 to 4 and the state space of Markov models before and after decomposition are shown in Table III. In the simulation, we generate Rayleigh fading channels by the Jakes Model using a U-shape Doppler power spectrum [33] for every pair of transmitter and receiver. In each simulated time slot, packets arrive to every queue according to Poisson distribution with mean $\lambda\Delta T$. For those D2D links with non-empty queues, we derive their respective SINR values in this time slot according to (2), where the channel gains of the D2D

TABLE III
STATE SPACE, ITERATIONS, AND RUNTIME WITH DIFFERENT NUMBER OF D2D LINKS

D	State space		Iters	Runtime (s)	
	original	decomposed		Numerics	Simulation
2	1.632e3	816	4	18	334 ($\lambda = 1$k) 970 ($\lambda = 100$k)
3	1.332e6	816	4	25	657 ($\lambda = 1$k) 1738 ($\lambda = 100$k)
4	1.086e9	816	5	34	1136 ($\lambda = 1$k) 2400 ($\lambda = 100$k)

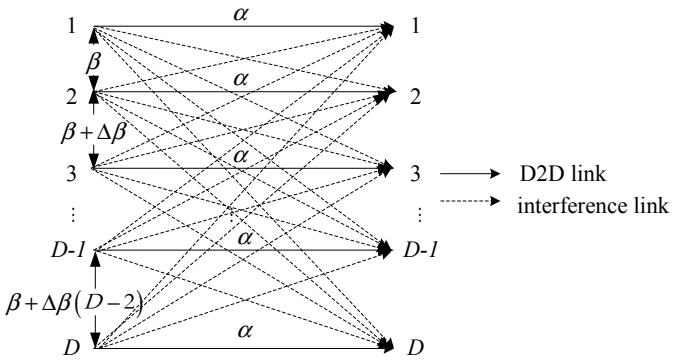

Fig. 6. The Network Topology. The distance between the transmitter and receiver of a link is denoted as α. The distance between the pair of transmitters (resp. receivers) of link i and $i+1$ is $\beta + \Delta\beta(i-1)$.

links and interfering links are generated by the Jakes Model. The corresponding transmission rates for the derived SINR values in this time slot can thus be derived according to Table II. The simulations are run over 10^5 time slots and the time-average performance measures of every D2D link are obtained. The simulation runtime is given in Table III which varies with both packet arrival rate λ and D2D link number D. In the numerical method, we set the initial steady-state probability vector $\boldsymbol{\pi}_i$ of every link i to be $\{\frac{1}{(K+1)\times L}, \ldots, \frac{1}{(K+1)\times L}\}$, and the initial vector of iteration variables $\{\mathbf{x}_1^0, \ldots, \mathbf{x}_D^0\}$ can be derived from (27). The number of iterations and runtime for convergence are given in Table III. It can be observed that the runtime for the iterative numerics is much shorter than the simulation runtime.

Fig.7(a)-7(d) show the mean queue length, mean throughput, mean delay and dropping probability averaged over all D2D links with varying arrival rates for D2D communications systems consisting of different numbers of links D, respectively. We choose $\alpha = 0.5$, $\beta = 0.3$ and $\Delta\beta = 0.01$. It can be seen that the numerical results match well with the simulation results under every configuration. As expected, the system performance in terms of all the above four measures degrade with the increasing number of links due to the growing amount of interference to every link. Fig.7(a) reveals that the mean queue length increases with the packet arrival rate and reaches the maximum buffer size 50 when the arrival rate reaches 100k packets/s. The variations of the mean throughput and dropping probability have a similar trend. Fig.7(b) shows that the difference in mean throughput when the numbers of links D are different grows larger with the increasing arrival rate. This is because the chances that the potential interfering links have data to transmit grow larger and thus the interference opportunities are increased for every link. The increase in mean throughput becomes insignificant when the arrival rate reaches 100k packets/s for every D. This is not surprising since it has almost reached the maximum transmission capacity of the system and the increasing arrival rate only results in increasing dropping probability. In Fig.7(d), it can be observed that the dropping probability is related to the maximum transmission capability of the system. Take $D = 4$ for example, the dropping probability reaches approximately 84% when the arrival rate is 100k packets/s, which means the system is overload by a factor of 5.2 (i.e., dropping probability/(1-dropping probability)). On the other hand, Fig.7(b) shows that the maximum transmission capability or the maximum mean throughput is 16k packets/s when $D = 4$, and 100k packets/s is indeed 5.2 times more than the maximum transmission capability of the system. Note that even in this saturated case, the amount of instantaneous interference received by a link can still be smaller than that under the infinite backlog traffic model, since the probability that the queue of any other link being empty cannot be zero as the Markov chain underlying the queuing system is irreducible. Fig.7(c) shows that the delay increases sharply when arrival rate increases from 1k packets/s to 20k packets/s, and then remains roughly the same when the arrival rate further increases. This is because when the arrival rate becomes larger than the maximum transmission capability of the system as discussed above, the system would have become overload if not for the packet dropping mechanism. Therefore, both the mean queue length and the mean throughput quickly reach their respective maximum values as revealed by Fig.7(a) and Fig.7(b). By Little's Law, the mean delay also remains the same after that.

Fig.8(a)-8(d) show the performance metrics with varying interference link length, where β ranges from 0.1 to 0.7 and the values of α and $\Delta\beta$ remain the same as above. The arrival rate is assumed to be 20K packets/s. The analytical results and the simulation results are very close, both of which improve with the increasing interference link length and decreasing interference from the other links. Note that when the interference link length is large, the performance gap between the scenarios with different numbers of links become small, since the difference in the amount of received interference is small in these topologies.

In the above numerical and simulation experiments, we assume that the packets arrive one at a time (as opposed to arriving in batches) following the Poisson process. However, we can extend the presented queuing model with the Batch Bernoulli arrival process by setting $\Pr.(A_{i,t} = a)$ in (4) to be the probability mass function of a Binomial distribution. We illustrate the numerical and simulation results with respect to dropping probability for D2D communications systems consisting of different numbers D of D2D links under Batch Bernoulli arrival process in Fig.9 with varying mean packet arrival rate and in Fig.10 with varying interference link length. We observe that the numerical results match well with the simulation results. Moreover, comparisons between Fig.9 and Fig.7(d) and between Fig.10 and Fig.8(d) show that the dropping probability under Poisson arrival process and Batch

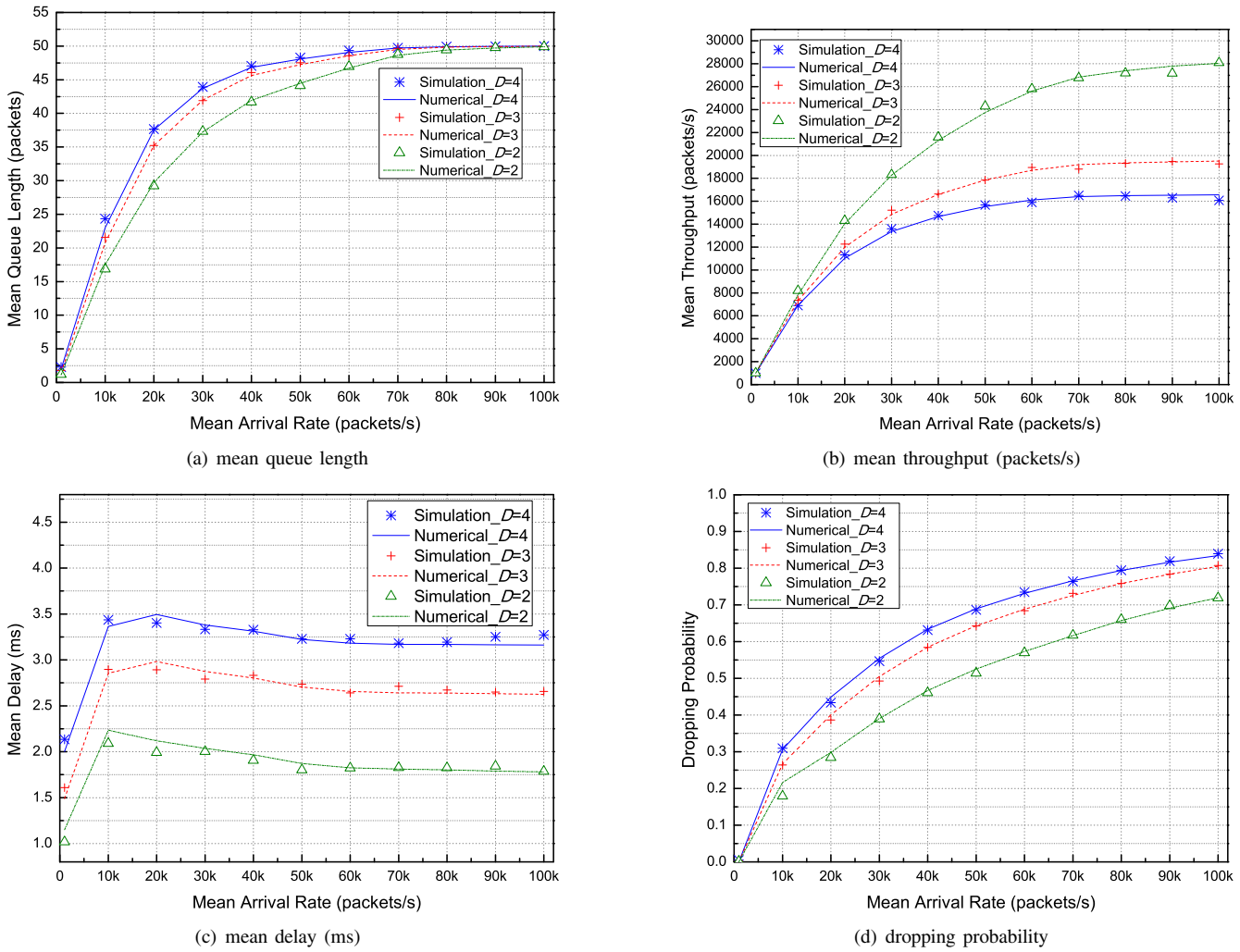

(a) mean queue length

(b) mean throughput (packets/s)

(c) mean delay (ms)

(d) dropping probability

Fig. 7. Performance metrics versus packet arrival rate for D2D communications systems consisting of different numbers D of D2D links ($\alpha = 0.5$, $\beta = 0.3$, and $\Delta\beta = 0.01$).

Bernoulli arrival process are quite similar.

VI. Conclusion and Future Work

In this paper, we have developed a numerical method to investigate the performance of D2D communications with frequency reuse between D2D links and dynamic data arrival with finite-length queuing. The system behavior is formulated by a coupled processor queuing model, where the service process is characterized by a FSMC with each state corresponding to a certain SINR interval. We first construct the underlying DTMC of the queuing model and compute the state transition probabilities of the DTMC to derive its steady-state distribution. Since the state space of the DTMC grows exponentially with link number, we next formulate a DSPN model of the queueing system and use the model decomposition and iteration techniques in SPN to derive the approximate steady-sate distribution of the DTMC with low complexity. Finally, we obtain the performance metrics of the D2D communications from the steady-state distribution of the DTMC, whose accuracy has been verified by simulation results.

In this paper, we focus on the narrowband communications scenario with flat fading wireless channels. When considering broadband communications scenario with frequency-selective fading channels, since the frequency-selective fading channels can be turned into multiple parallel flat fading channels by the Orthogonal Frequency Division Multiplex (OFDM) technique, the channel state space in our FSMC model may grow exponentially with the increasing number of flat fading channels corresponding to increasing system bandwidth. Therefore, we will expand our numerical method for frequency-selective fading channels using colored Stochastic Petri Nets for state aggregation. Furthermore, since we have provided both numerical methods for the two extreme cases of resource sharing between D2D links, i.e., full reuse and orthogonal sharing, we will develop efficient interference management schemes. In addition, we will study two cases in D2D communications system without making the assumption that a pair of source and destination D2D UEs always communicate via the same direct over-the-air link. The first case is that the D2D UEs support multi-hop transmission capability. Therefore, since there can be multiple routes for a flow with a fixed pair of source and destination UEs, the transmitting node has the option to select the channel on which the flow should be transmitted. The second case is when the dynamic D2D mode

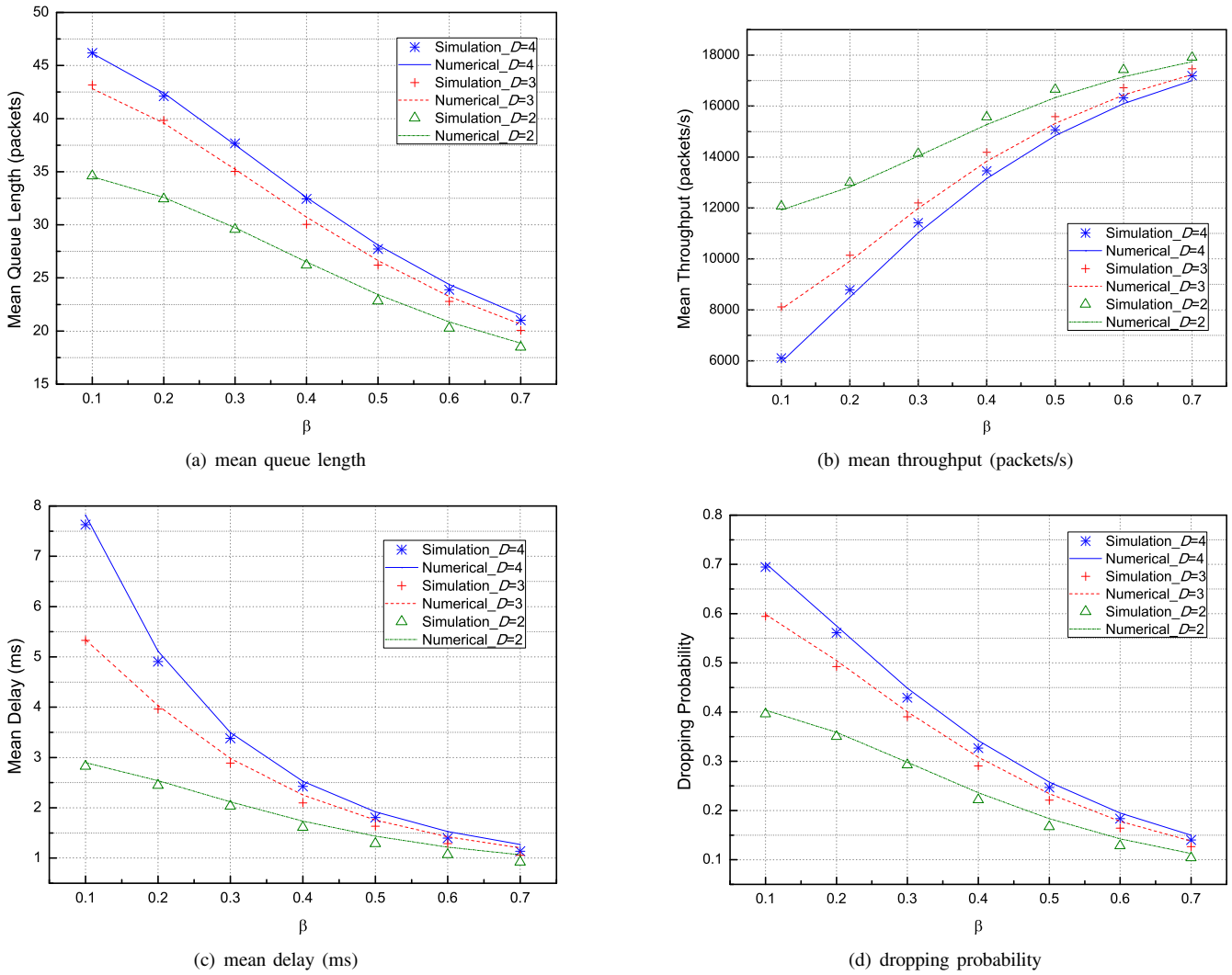

(a) mean queue length

(b) mean throughput (packets/s)

(c) mean delay (ms)

(d) dropping probability

Fig. 8. Performance metrics versus interference link length for D2D communications systems consisting of different numbers D of D2D links ($\alpha = 0.5$, $\Delta\beta = 0.01$, mean arrival rate is 20K packets/s. Since the length of the potential interfering link I_{ji} of link i, where $j > i$ (resp. $j < i$) and $i, j \in \mathcal{D}$, is $\sqrt{\alpha^2 + \left(\sum_{k=i}^{j-1}(\beta + \Delta\beta(k-1))\right)^2}$ (resp. $\sqrt{\alpha^2 + \left(\sum_{k=j}^{i-1}(\beta + \Delta\beta(k-1))\right)^2}$), the interference link length varies with β on the x-axis).

selection is considered, where the traffic between a pair of source and destination D2D UEs can be transmitted either via the D2D link or via the cellular uplink to the base station and then relayed via the cellular downlink to the destination UE. The research on both cases are interesting and challenging. Although we assume that the packets arrive one at a time following the Poisson process, only minor revision is needed to our numerical method if the packets arrive according to the Batch Bernoulli process as validated by simulation in Section V. Extension of our numerical method to more sophisticated arrival processes such as the Batch Markovian arrival process (BMAP) will be studied. Finally, it is interesting in applying our numerical method to the performance evaluation of other dynamic interference scenarios, e.g., wireless networks with multiple base stations.

APPENDIX

A. Calculation of the integration in (20)

Given $\{\hat{\Theta}_j\}_{j\in\mathcal{D}\backslash\{i\}} = \theta_v$, $\{\Theta_j\}_{j\in\mathcal{D}\backslash\{i\}} = \theta_w$ and $v \neq w$, we define $\mathcal{I}_i^v := \{I_{ji} | j \in \mathcal{D}\backslash\{i\} : \hat{\Theta}_j = 1\}$ as the subset of interfering links I_{ji} with $\hat{\Theta}_j = 1$, and $\mathcal{I}_i^w := \{I_{ji} | j \in \mathcal{D}\backslash\{i\} : \Theta_j = 1\}$ as the subset of interfering links I_{ji} with $\Theta_j = 1$. Furthermore, we define $\mathcal{I}_i^{vw} := \mathcal{I}_i^v \bigcap \mathcal{I}_i^w$, which could be an empty set $\emptyset$. Finally, we define $\mathcal{I}_i^{v\bar{w}} := \mathcal{I}_i^v \backslash \mathcal{I}_i^{vw}$ and $\mathcal{I}_i^{\bar{v}w} := \mathcal{I}_i^w \backslash \mathcal{I}_i^{vw}$, which are the difference of subsets $\mathcal{I}_i^v$ and $\mathcal{I}_i^w$ and the difference of subsets $\mathcal{I}_i^w$ and $\mathcal{I}_i^v$, respectively. Since $\mathcal{I}_i^v \neq \mathcal{I}_i^w$, the relationship between $\mathcal{I}_i^v$ and $\mathcal{I}_i^w$ can be divided into the following four mutually exclusive and exhaustive cases, as shown in Fig.(11):

1) $\mathcal{I}_i^v = \emptyset$ or $\mathcal{I}_i^w = \emptyset$, and in both subcases, $\mathcal{I}_i^{vw} = \emptyset$; in the former subcase, we have $\mathcal{I}_i^{v\bar{w}} = \emptyset$, while in the latter subcase, we have $\mathcal{I}_i^{\bar{v}w} = \emptyset$; in the following three cases, we implicitly assume that $\mathcal{I}_i^v \neq \emptyset$ and $\mathcal{I}_i^w \neq \emptyset$;
2) $\mathcal{I}_i^v \subset \mathcal{I}_i^w$ or $\mathcal{I}_i^w \subset \mathcal{I}_i^v$, and in the former subcase, we have $\mathcal{I}_i^{vw} = \mathcal{I}_i^v$, $\mathcal{I}_i^{v\bar{w}} = \emptyset$, while in the latter subcase, we have $\mathcal{I}_i^{vw} = \mathcal{I}_i^w$, $\mathcal{I}_i^{\bar{v}w} = \emptyset$;
3) $\mathcal{I}_i^v \bigcap \mathcal{I}_i^w = \mathcal{I}_i^{vw} = \emptyset$, and in this case, we have $\mathcal{I}_i^{v\bar{w}} = \mathcal{I}_i^v$ and $\mathcal{I}_i^{\bar{v}w} = \mathcal{I}_i^w$;
4) $\mathcal{I}_i^v \not\subseteq \mathcal{I}_i^w$, $\mathcal{I}_i^w \not\subseteq \mathcal{I}_i^v$, and $\mathcal{I}_i^{vw} \neq \emptyset$, and in this case, we have $\mathcal{I}_i^{v\bar{w}} \neq \emptyset$ and $\mathcal{I}_i^{\bar{v}w} \neq \emptyset$.

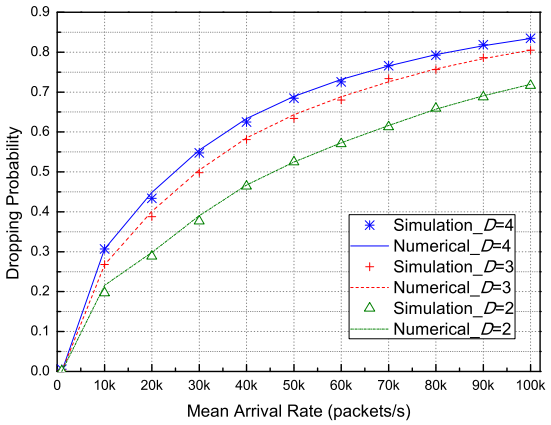

Fig. 9. Dropping probability versus packet arrival rate for D2D communications systems consisting of different numbers D of D2D links under Batch Bernoulli arrival process ($\alpha = 0.5$, $\beta = 0.3$, and $\Delta\beta = 0.01$).

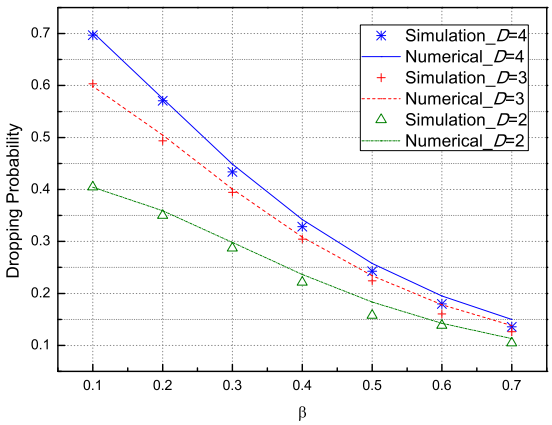

Fig. 10. Dropping probability versus interference link length for D2D communications systems consisting of different numbers D of D2D links under Batch Bernoulli arrival process ($\alpha = 0.5$, $\Delta\beta = 0.01$, mean arrival rate is 20K packets/s. Since the length of the potential interfering link I_{ji} of link i, where $j > i$ (resp. $j < i$) and $i, j \in \mathcal{D}$, is $\sqrt{\alpha^2 + \left(\sum_{k=i}^{j-1}(\beta + \Delta\beta(k-1))\right)^2}$ (resp. $\sqrt{\alpha^2 + \left(\sum_{k=j}^{i-1}(\beta + \Delta\beta(k-1))\right)^2}$), the interference link length varies with β on the x-axis).

Denote the index set of $\mathcal{I}_i^{vw}$ as $\mathcal{J}^1$, i.e., $\mathcal{I}_i^{vw} = \{I_{ji}\}_{j\in\mathcal{J}^1}$. Similarly, denote the index sets of $\mathcal{I}_i^{v\bar{w}}$ and $\mathcal{I}_i^{\bar{v}w}$ as $\mathcal{J}^2$ and $\mathcal{J}^3$, respectively. In (19), the integration region of $\vec{\gamma}_i$ needs to obey the following constraints.

$$\begin{aligned} \chi_{(l_i-1)} \leq & \frac{\gamma_{ii}}{1+\sum_{j\in\mathcal{J}^1}\gamma_{ji}+\sum_{j\in\mathcal{J}^2}\gamma_{ji}} < \chi_{l_i}, \\ \chi_{(n_i-1)} \leq & \frac{\gamma_{ii}}{1+\sum_{j\in\mathcal{J}^1}\gamma_{ji}+\sum_{j\in\mathcal{J}^3}\gamma_{ji}} < \chi_{n_i}, \\ & \vec{\gamma}_i \geq 0. \end{aligned} \tag{38}$$

Let $\gamma s_1 := \sum_{j\in\mathcal{J}^1}\gamma_{ji}$, $\gamma s_2 := \sum_{j\in\mathcal{J}^2}\gamma_{ji}$, and $\gamma s_3 := \sum_{j\in\mathcal{J}^3}\gamma_{ji}$, which are all sum of independent exponential random variables. The pdf of $\gamma s_{id}, id = 1,2,3$ has closed form expression as

$$f_{\gamma s_{id}}(x) = [\prod_{j\in\mathcal{J}^{id}}\frac{1}{\bar{\gamma}_{ji}}]\sum_{j\in\mathcal{J}^{id}}\frac{\exp(-x/\bar{\gamma}_{ji})}{\prod_{k\in\mathcal{J}^{id}\setminus\{j\}}(1/\bar{\gamma}_{ki}-1/\bar{\gamma}_{ji})}, \tag{39}$$

if $\{\gamma_{ji}\}_{j\in\mathcal{J}^{id}}$ have pairwise distinct mean $\bar{\gamma}_{ji}$.

Remark 1: Since the D2D terminals are randomly distributed in the cell in practical communications system, the probability that two D2D links have exactly the same mean SNR value is small. Therefore, the assumption that $\{\gamma_{ji}\}_{j\in\mathcal{J}^{id}}$ have pairwise distinct mean $\bar{\gamma}_{ji}$ is reasonable. Even if two D2D links do have the same mean SNR, we can add a very small number to one of the SNR to make the two values different, which will not have much impact on the performance evaluation results.

Now we try to calculate the integration in (20) under each of the four cases listed above.

1) Case 1: We consider that $\mathcal{I}_i^v = \emptyset$, while the subcase of $\mathcal{I}_i^w = \emptyset$ can be dealt with by a similar method. In this case, the polyhedron in (38) is equivalent to

$$\begin{aligned} \chi_{(l_i-1)} \leq & \gamma_{ii} < \chi_{l_i}, \\ \chi_{(n_i-1)} \leq & \frac{\gamma_{ii}}{1+\gamma s_3} < \chi_{n_i}, \\ & \gamma_{ii} \geq 0,\ \gamma s_3 \geq 0. \end{aligned} \tag{40}$$

which in turn is equivalent to

$$\begin{aligned} \chi_{(l_i-1)} \leq & \gamma_{ii} < \chi_{l_i}, \\ \max\{0, \frac{\gamma_{ii}}{\chi_{n_i}} - 1\} \leq & \gamma s_3 < \frac{\gamma_{ii}}{\chi_{(n_i-1)}} - 1, \end{aligned} \tag{41}$$

2) Case 2: We consider that $\mathcal{I}_i^v \subset \mathcal{I}_i^w$, while the subcase of $\mathcal{I}_i^w \subset \mathcal{I}_i^v$ can be dealt with by a similar method. In this case, the polyhedron in (38) is equivalent to

$$\begin{aligned} \chi_{(l_i-1)} \leq & \frac{\gamma_{ii}}{1+\gamma s_1} < \chi_{l_i}, \\ \chi_{(n_i-1)} \leq & \frac{\gamma_{ii}}{1+\gamma s_1+\gamma s_3} < \chi_{n_i}, \\ & \gamma_{ii} \geq 0,\ \gamma s_1 \geq 0,\ \gamma s_3 \geq 0. \end{aligned} \tag{42}$$

which in turn is equivalent to

$$\begin{aligned} \chi_{(l_i-1)} \leq & \gamma_{ii}, \\ \max\{0, \frac{\gamma_{ii}}{\chi_{l_i}} - 1\} \leq & \gamma s_1 < \frac{\gamma_{ii}}{\chi_{(l_i-1)}} - 1, \\ \max\{0, \frac{\gamma_{ii}}{\chi_{n_i}} - \gamma s_1 - 1\} \leq & \gamma s_3 < \frac{\gamma_{ii}}{\chi_{(n_i-1)}} - \gamma s_1 - 1. \end{aligned} \tag{43}$$

3) Case 3: In this case, the polyhedron in (38) is equivalent to

$$\begin{aligned} \chi_{(l_i-1)} \leq & \frac{\gamma_{ii}}{1+\gamma s_2} < \chi_{l_i}, \\ \chi_{(n_i-1)} \leq & \frac{\gamma_{ii}}{1+\gamma s_3} < \chi_{n_i}, \\ & \gamma_{ii} \geq 0,\ \gamma s_2 \geq 0,\ \gamma s_3 \geq 0. \end{aligned} \tag{44}$$

which in turn is equivalent to

$$\begin{aligned} \max\{\chi_{(l_i-1)}, \chi_{(n_i-1)}\} \leq & \gamma_{ii}, \\ \max\{0, \frac{\gamma_{ii}}{\chi_{l_i}} - 1\} \leq & \gamma s_2 < \frac{\gamma_{ii}}{\chi_{(l_i-1)}} - 1, \\ \max\{0, \frac{\gamma_{ii}}{\chi_{n_i}} - 1\} \leq & \gamma s_3 < \frac{\gamma_{ii}}{\chi_{(n_i-1)}} - 1. \end{aligned} \tag{45}$$

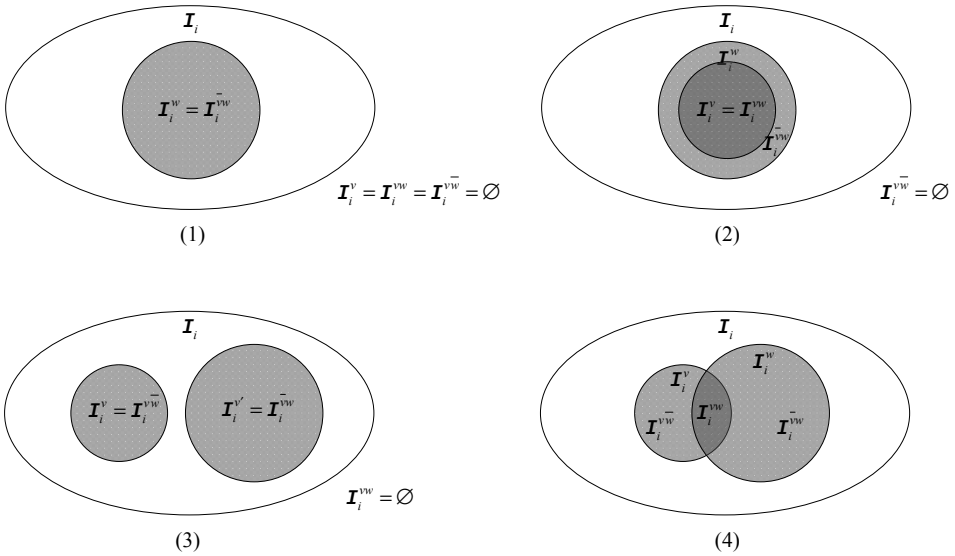

Fig. 11. The interfering link set.

4) Case 4: In this case, the polyhedron in (38) is equivalent to

$$\begin{aligned}\chi_{(l_i-1)} \leq& \frac{\gamma_{ii}}{1+\gamma s_1+\gamma s_2} < \chi_{l_i},\\ \chi_{(n_i-1)} \leq& \frac{\gamma_{ii}}{1+\gamma s_1+\gamma s_3} < \chi_{n_i},\\ \gamma_{ii} \geq 0,\ \gamma s_1 \geq 0,\ \gamma s_2 \geq 0,\ \gamma s_3 \geq 0.& \end{aligned} \tag{46}$$

which in turn is equivalent to

$$\begin{aligned}\max\{\chi_{(l_i-1)}, \chi_{(n_i-1)}\} \leq& \gamma_{ii},\\ \max\{0, \frac{\gamma_{ii}}{\chi_{l_i}} - \gamma s_1 - 1\} \leq& \gamma s_2 < \frac{\gamma_{ii}}{\chi_{(l_i-1)}} - \gamma s_1 - 1,\\ \max\{0, \frac{\gamma_{ii}}{\chi_{n_i}} - \gamma s_1 - 1\} \leq& \gamma s_3 < \frac{\gamma_{ii}}{\chi_{(n_i-1)}} - \gamma s_1 - 1,\\ 0 \leq& \gamma s_1 < \min\{\frac{\gamma_{ii}}{\chi_{(l_i-1)}} - 1, \frac{\gamma_{ii}}{\chi_{(n_i-1)}} - 1\}.\end{aligned} \tag{47}$$

In all the above cases, we try to have the integration limits of γ_{ii}, γs_1, γs_2, and γs_3 as affine functions. Since Case 4 is the most complex one and the other cases can be considered as special circumstances of Case 4, we will only discuss the integration of (20) under Case 4 in details due to space limitation.

1) If $l_i = n_i$,
   - and if $\chi_{(l_i-1)} \leq \gamma_{ii} < \chi_{l_i}$, we have $A1$ equals

$$\begin{aligned}&\int_{\chi_{(l_i-1)}}^{\chi_{l_i}} f(\gamma_{ii})\mathrm{d}\gamma_{ii} \int_0^{\frac{\gamma_{ii}}{\chi_{(l_i-1)}}-1} f_{\gamma s_1}(\gamma s_1)\mathrm{d}\gamma s_1\\ &\int_0^{\frac{\gamma_{ii}}{\chi_{(l_i-1)}}-\gamma s_1-1} f_{\gamma s_2}(\gamma s_2)\mathrm{d}\gamma s_2 \int_0^{\frac{\gamma_{ii}}{\chi_{(l_i-1)}}-\gamma s_1-1}\\ &f_{\gamma s_3}(\gamma s_3)\mathrm{d}\gamma s_3,\end{aligned} \tag{48}$$

   - and if $\gamma_{ii} \geq \chi_{l_i}$, $\gamma s_1 \geq \frac{\gamma_{ii}}{\chi_{l_i}} - 1$, we have $A2$ equals

$$\begin{aligned}&\int_{\chi_{l_i}}^{\infty} f(\gamma_{ii})\mathrm{d}\gamma_{ii} \int_{\frac{\gamma_{ii}}{\chi_{l_i}}-1}^{\frac{\gamma_{ii}}{\chi_{(l_i-1)}}-1}\\ &f_{\gamma s_1}(\gamma s_1)\mathrm{d}\gamma s_1 \int_0^{\frac{\gamma_{ii}}{(\chi_{l_i-1)}}-\gamma s_1-1}\\ &f_{\gamma s_2}(\gamma s_2)\mathrm{d}\gamma s_2 \int_0^{\frac{\gamma_{ii}}{(\chi_{l_i-1)}}-\gamma s_1-1} f_{\gamma s_3}(\gamma s_3)\mathrm{d}\gamma s_3,\end{aligned} \tag{49}$$

   - else if $\gamma_{ii} \geq \chi_{l_i}$, $\gamma s_1 < \frac{\gamma_{ii}}{\chi_{l_i}} - 1$, we have $A3$ equals

$$\int_{\chi_{l_i}}^{\infty} f(\gamma_{ii})\mathrm{d}\gamma_{ii} \int_0^{\frac{\gamma_{ii}}{\chi_{l_i}}-1} \tag{50}$$

2) If $l_i > n_i$,
   - and if $\chi_{(l_i-1)} \leq \gamma_{ii} < \chi_{l_i}$, we have $A1$ equals

$$\begin{aligned}&\int_{\chi_{(l_i-1)}}^{\chi_{l_i}} f(\gamma_{ii})\mathrm{d}\gamma_{ii} \int_0^{\frac{\gamma_{ii}}{\chi_{(l_i-1)}}-1} f_{\gamma s_1}(\gamma s_1)\mathrm{d}\gamma s_1\\ &\int_0^{\frac{\gamma_{ii}}{\chi_{(l_i-1)}}-\gamma s_1-1} f_{\gamma s_2}(\gamma s_2)\mathrm{d}\gamma s_2 \int_{\frac{\gamma_{ii}}{\chi_{n_i}}-\gamma s_1-1}^{\frac{\gamma_{ii}}{\chi_{(n_i-1)}}-\gamma s_1-1}\\ &f_{\gamma s_3}(\gamma s_3)\mathrm{d}\gamma s_3,\end{aligned} \tag{51}$$

   - and if $\gamma_{ii} \geq \chi_{l_i}$, $\gamma s_1 \geq \frac{\gamma_{ii}}{\chi_{l_i}} - 1$, we have $A2$ equals

$$\begin{aligned}&\int_{\chi_{l_i}}^{\infty} f(\gamma_{ii})\mathrm{d}\gamma_{ii} \int_{\frac{\gamma_{ii}}{\chi_{l_i}}-1}^{\frac{\gamma_{ii}}{\chi_{(l_i-1)}}-1} f_{\gamma s_1}(\gamma s_1)\mathrm{d}\gamma s_1\\ &\int_0^{\frac{\gamma_{ii}}{\chi_{(l_i-1)}}-\gamma s_1-1}\\ &f_{\gamma s_2}(\gamma s_2)\mathrm{d}\gamma s_2 \int_{\frac{\gamma_{ii}}{\chi_{n_i}}-\gamma s_1-1}^{\frac{\gamma_{ii}}{\chi_{(n_i-1)}}-\gamma s_1-1} f_{\gamma s_3}(\gamma s_3)\mathrm{d}\gamma s_3,\end{aligned} \tag{52}$$

- else if $\gamma_{ii} \geq \chi_{l_i}$, $\gamma s_1 < \frac{\gamma_{ii}}{\chi_{l_i}} - 1$, we have $A3$ equals

$$\int_{\chi_{l_i}}^{\infty} f(\gamma_{ii})\mathrm{d}\gamma_{ii} \int_{0}^{\frac{\gamma_{ii}}{\chi_{l_i}}-1} f_{\gamma s_1}(\gamma s_1)\mathrm{d}\gamma s_1 \int_{\frac{\gamma_{ii}}{\chi_{(l_i-1)}}-\gamma s_1-1}^{\frac{\gamma_{ii}}{\chi_{(l_i-1)}}-\gamma s_1-1} f_{\gamma s_2}(\gamma s_2)\mathrm{d}\gamma s_2 \int_{\frac{\gamma_{ii}}{\chi_{n_i}}-\gamma s_1-1}^{\frac{\gamma_{ii}}{\chi_{(n_i-1)}}-\gamma s_1-1} f_{\gamma s_3}(\gamma s_3)\mathrm{d}\gamma s_3. \quad (53)$$

3) If $l_i < n_i$,

- and if $\chi_{(n_i-1)} \leq \gamma_{ii} < \chi_{n_i}$, we have $A1$ equals

$$\int_{\chi_{(n_i-1)}}^{\chi_{n_i}} f(\gamma_{ii})\mathrm{d}\gamma_{ii} \int_{0}^{\frac{\gamma_{ii}}{\chi_{(n_i-1)}}-1} f_{\gamma s_1}(\gamma s_1)\mathrm{d}\gamma s_1 \int_{\frac{\gamma_{ii}}{\chi_{(l_i-1)}}-\gamma s_1-1}^{\frac{\gamma_{ii}}{\chi_{(l_i-1)}}-\gamma s_1-1} f_{\gamma s_2}(\gamma s_2)\mathrm{d}\gamma s_2 \int_{0}^{\frac{\gamma_{ii}}{\chi_{(n_i-1)}}-\gamma s_1-1} f_{\gamma s_3}(\gamma s_3)\mathrm{d}\gamma s_3, \quad (54)$$

- and if $\gamma_{ii} \geq \chi_{n_i}$, $\gamma s_1 \geq \frac{\gamma_{ii}}{\chi_{n_i}} - 1$, we have $A2$ equals

$$\int_{\chi_{n_i}}^{\infty} f(\gamma_{ii})\mathrm{d}\gamma_{ii} \int_{\frac{\gamma_{ii}}{\chi_{n_i}}-1}^{\frac{\gamma_{ii}}{\chi_{(n_i-1)}}-1} f_{\gamma s_1}(\gamma s_1)\mathrm{d}\gamma s_1 \int_{\frac{\gamma_{ii}}{\chi_{(l_i-1)}}-\gamma s_1-1}^{\frac{\gamma_{ii}}{\chi_{(l_i-1)}}-\gamma s_1-1} f_{\gamma s_2}(\gamma s_2)\mathrm{d}\gamma s_2 \int_{0}^{\frac{\gamma_{ii}}{\chi_{(n_i-1)}}-\gamma s_1-1} f_{\gamma s_3}(\gamma s_3)\mathrm{d}\gamma s_3, \quad (55)$$

- else if $\gamma_{ii} \geq \chi_{n_i}$, $\gamma s_1 < \frac{\gamma_{ii}}{\chi_{n_i}} - 1$, we have $A3$ equals

$$\int_{\chi_{n_i}}^{\infty} f(\gamma_{ii})\mathrm{d}\gamma_{ii} \int_{0}^{\frac{\gamma_{ii}}{\chi_{n_i}}-1} f_{\gamma s_1}(\gamma s_1)\mathrm{d}\gamma s_1 \int_{\frac{\gamma_{ii}}{\chi_{(l_i-1)}}-\gamma s_1-1}^{\frac{\gamma_{ii}}{\chi_{(l_i-1)}}-\gamma s_1-1} f_{\gamma s_2}(\gamma s_2)\mathrm{d}\gamma s_2 \int_{\frac{\gamma_{ii}}{\chi_{n_i}}-\gamma s_1-1}^{\frac{\gamma_{ii}}{\chi_{(n_i-1)}}-\gamma s_1-1} f_{\gamma s_3}(\gamma s_3)\mathrm{d}\gamma s_3. \quad (56)$$

Therefore, $\hat{p}_{(\theta_v,\theta_w)}^{l_i+1,n_i} = A1 + A2 + A3$ when $l_i = n_i$, $l_i > n_i$, and $l_i < n_i$, respectively. Combining (39) with the above integrations, and after mathematical manipulation, we have:

1) if $l_i = n_i$,

$$\hat{p}_{(\theta_v,\theta_w)}^{l_i,n_i} = \frac{1}{\bar{\gamma}_{ii}}[\prod_{j\in\mathcal{J}^1}\frac{1}{\bar{\gamma}_{ji}}][\prod_{j'\in\mathcal{J}^2}\frac{1}{\bar{\gamma}_{j'i}}][\prod_{j''\in\mathcal{J}^3}\frac{1}{\bar{\gamma}_{j''i}}]\sum_{j\in\mathcal{J}^1}\sum_{j'\in\mathcal{J}^2}\sum_{j''\in\mathcal{J}^3}\frac{\bar{\gamma}_{j'i}\bar{\gamma}_{j''i}(F(\chi_{(l_i-1)}) - F(\chi_{l_i}))}{\prod_{k\in\mathcal{J}^1\setminus\{j\}}[\frac{1}{\bar{\gamma}_{ki}} - \frac{1}{\bar{\gamma}_{ji}}]\prod_{k'\in\mathcal{J}^2\setminus\{j'\}}[\frac{1}{\bar{\gamma}_{k'i}} - \frac{1}{\bar{\gamma}_{j'i}}]}\frac{1}{\prod_{k''\in\mathcal{J}^3\setminus\{j''\}}[\frac{1}{\bar{\gamma}_{k''i}} - \frac{1}{\bar{\gamma}_{j''i}}]}, \quad (57)$$

where

$$F(a) = \frac{\exp(\frac{-a}{\bar{\gamma}_{ii}})\bar{\gamma}_{ii}^4\bar{\gamma}_{ji}(2a\bar{\gamma}_{j'i}\bar{\gamma}_{j''i} + \bar{\gamma}_{ii}(\bar{\gamma}_{j'i} + \bar{\gamma}_{j''i}))}{(\bar{\gamma}_{ii} + a\bar{\gamma}_{ji})(\bar{\gamma}_{ii} + a\bar{\gamma}_{j'i})(\bar{\gamma}_{ii} + a\bar{\gamma}_{j''i})} \times \frac{1}{(a\bar{\gamma}_{j'i}\bar{\gamma}_{j''i} + \bar{\gamma}_{ii}(\bar{\gamma}_{j'i} + \bar{\gamma}_{j''i}))}; \quad (58)$$

2) if $l_i > n_i$,

$$\hat{p}_{(\theta_v,\theta_w)}^{l_i,n_i} = \frac{1}{\bar{\gamma}_{ii}}[\prod_{j\in\mathcal{J}^1}\frac{1}{\bar{\gamma}_{ji}}][\prod_{j'\in\mathcal{J}^2}\frac{1}{\bar{\gamma}_{j'i}}][\prod_{j''\in\mathcal{J}^3}\frac{1}{\bar{\gamma}_{j''i}}] \sum_{j\in\mathcal{J}^1}\sum_{j'\in\mathcal{J}^2}\sum_{j''\in\mathcal{J}^3} \frac{\bar{\gamma}_{j'i}\bar{\gamma}_{j''i}\exp(\frac{1}{\bar{\gamma}_{j''i}})}{\prod_{k\in\mathcal{J}^1\setminus\{j\}}[\frac{1}{\bar{\gamma}_{ki}} - \frac{1}{\bar{\gamma}_{ji}}]\prod_{k'\in\mathcal{J}^2\setminus\{j'\}}[\frac{1}{\bar{\gamma}_{k'i}} - \frac{1}{\bar{\gamma}_{j'i}}]} \frac{1}{\prod_{k''\in\mathcal{J}^3\setminus\{j''\}}[\frac{1}{\bar{\gamma}_{k''i}} - \frac{1}{\bar{\gamma}_{j''i}}]}(F'(\chi_{n_i},\chi_{(l_i-1)}) - F'(\chi_{(n_i-1)},\chi_{(l_i-1)}) - F'(\chi_{n_i},\chi_{l_i}) + F'(\chi_{(n_i-1)},\chi_{l_i})), \quad (59)$$

where

$$F'(a,b) = \frac{\exp(-b(\frac{1}{a\bar{\gamma}_{j''i}} + \frac{1}{\bar{\gamma}_{ii}}))a^3\bar{\gamma}_{ii}^3\bar{\gamma}_{ji}\bar{\gamma}_{j''i}^3}{(\bar{\gamma}_{ii} + a\bar{\gamma}_{j''i})(a\bar{\gamma}_{ii}\bar{\gamma}_{j''i} + b\bar{\gamma}_{j'i}(\bar{\gamma}_{ii} + a\bar{\gamma}_{j''i}))} \times \frac{1}{(b\bar{\gamma}_{ii}\bar{\gamma}_{ji} + a(b\bar{\gamma}_{ji}\bar{\gamma}_{j''i} + \bar{\gamma}_{ii}(\bar{\gamma}_{j''i} - \bar{\gamma}_{ji})))} \quad (60)$$

3) if $l_i < n_i$, $\hat{p}_{(\theta_v,\theta_w)}^{l_i,n_i}$ can be derived according to (59) except that $\chi_{(n_i-1)}$ (resp. χ_{n_i}) and $\chi_{(l_i-1)}$ (resp. χ_{l_i}) switch places with each other.

Although we will not discuss the integration of (20) in case 1, 2 and 3 in detail, we will prove the following Lemma, which will be used in Appendix B for the prove of Theorem 3.

Lemma 1: In Case 1 and Case 2, $\hat{p}_{(\theta_v,\theta_w)}^{l_i,n_i} > 0$ for any $l_i, n_i \in \{1,\ldots,L\}$ satisfying $l_i \geq n_i$ (resp. $l_i \leq n_i$) when $\mathcal{I}_i^v \subset \mathcal{I}_i^w$ (resp. $\mathcal{I}_i^w \subset \mathcal{I}_i^v$); In Case 3 and Case 4, $\hat{p}_{(\theta_v,\theta_w)}^{l_i,n_i} > 0$ for any $l_i, n_i \in \{1,\ldots,L\}$.

Proof: In order to prove $\hat{p}_{(\theta_v,\theta_w)}^{l_i,n_i} > 0$, we need to show that the integration region $\Upsilon_{l_i} \bigcap \Upsilon_{n_i}$ is non-empty according to (20).

- In case 1, since (41) defines the integration region when $\mathcal{I}_i^v \subset \mathcal{I}_i^w$, we need to verify that for any $l_i, n_i \in \{1,\ldots,L\}$ satisfying $l_i \geq n_i$, the upper limit of integration for γs_3 is not always smaller than its lower limits when $\gamma_{ii} \in [\chi_{(l_i-1)}, \chi_{l_i})$. In (41), if $l_i \geq n_i$, we have $\gamma_{ii} \geq \chi_{(l_i-1)} \geq \chi_{(n_i-1)}$. Therefore, the upper limits of integration for γs_3, i.e., $\frac{\gamma_{ii}}{\chi_{(n_i-1)}} - 1$ is larger than zero when $\gamma_{ii} > \chi_{(n_i-1)}$, and thus larger than the lower limits of integration for γs_3, i.e., $\max\{0, \frac{\gamma_{ii}}{\chi_{n_i}} - 1\}$. The scenario when $\mathcal{I}_i^w \subset \mathcal{I}_i^v$ can be proved in a similar way.
- In case 2, since (43) defines the integration region when $\mathcal{I}_i^v \subset \mathcal{I}_i^w$, we need to verify that for any $l_i, n_i \in \{1,\ldots,L\}$ satisfying $l_i \geq n_i$, the upper limits of integration for γs_1 and γs_3 are not always smaller than their corresponding lower limits when $\gamma_{ii} \in [\chi_{(l_i-1)}, \infty)$. In

(43), the upper limit of γs_1, i.e, $\frac{\gamma_{ii}}{\chi_{(l_i-1)}}-1$ is larger than zero when $\gamma_{ii} > \chi_{(l_i-1)}$, and thus larger than the lower limits of integration for γs_1, i.e., $\max\{0, \frac{\gamma_{ii}}{\chi_{l_i}}-1\}$. Furthermore, since $l_i \geq n_i$ and $\gamma s_1 < \frac{\gamma_{ii}}{\chi_{(l_i-1)}}-1$, the upper limits of integration for γs_3, i.e., $\frac{\gamma_{ii}}{\chi_{(n_i-1)}}-\gamma s_1-1$ is larger than zero, and thus larger than the lower limits of integration for γs_3, i.e., $\max\{0, \frac{\gamma_{ii}}{\chi_{n_i}}-\gamma s_1-1\}$. The scenario when $\mathcal{I}_i^w \subset \mathcal{I}_i^v$ can be proved in a similar way.

- In case 3, since (45) defines the integration region, we need to verify that for any $l_i, n_i \in \{1,\ldots,L\}$, the upper limits of integration for γs_2 and γs_3 are not always smaller than their corresponding lower limits when $\gamma_{ii} \in [\max\{\chi_{(l_i-1)}, \chi_{(n_i-1)}\}, \infty)$. In (45), the upper limits of integration for γs_2 and γs_3, i.e, $\frac{\gamma_{ii}}{\chi_{(l_i-1)}}-1$ and $\frac{\gamma_{ii}}{\chi_{(n_i-1)}}-1$ are larger than zero when $\gamma_{ii} > \max\{\chi_{(l_i-1)}, \chi_{(n_i-1)}\}$, and thus larger than their corresponding lower limits of integration, i.e., $\max\{0, \frac{\gamma_{ii}}{\chi_{l_i}}-1\}$ and $\max\{0, \frac{\gamma_{ii}}{\chi_{n_i}}-1\}$.
- In case 4, since A_1, A_2 and A_3 are all larger than zero when $l_i > n_i$, $l_i < n_i$ and $l_i = n_i$, $\hat{p}^{l_i,n_i}_{(\theta_v,\theta_w)} = A_1 + A_2 + A_3 > 0$ for any $l_i, n_i \in \{1,\ldots,L\}$.

■

B. Proof of Theorem 3

We first prove the following lemmas.

Lemma 2: The Markov chain $(\vec{H}_t, \vec{Q}_t)$ is irreducible, if $K \leq R_L \Delta T$.

Proof: We can prove Lemma 2 by showing that for each transition from state $(\vec{l},\vec{k})$ to $(\vec{n},\vec{h})$, there exists a multi-transition path with non-zero probability, which is denoted as $(\vec{l},\vec{k}) \longrightarrow (\vec{n},\vec{h})$. Now we shall verify the following cases:

1) $(\vec{l},\vec{k}) \longrightarrow (\vec{l^*},\vec{k})$, for any $\vec{l^*} = \{l_i^* \in \{1,\ldots,L\} : R_{l_i^*}\Delta T \geq k_i\}_{i\in\mathcal{D}}$.
   - First, we will prove that $p^{\{l_i+1\}_{i\in\mathcal{D}}}_{(\vec{l},\vec{k},\vec{k})} > 0$, $p^{\{l_i-1\}_{i\in\mathcal{D}}}_{(\vec{l},\vec{k},\vec{k})} > 0$ and $p^{\vec{l}}_{(\vec{l},\vec{k},\vec{k})} > 0$. From (23), we only need to prove that $p^{(l_i+1)}_{(l_i,\vec{k},\vec{k})} > 0$, $p^{(l_i-1)}_{(l_i,\vec{k},\vec{k})} > 0$, and $p^{l_i}_{(l_i,\vec{k},\vec{k})} > 0$. According to Theorem 1, this is equivalent to proving that $p^{(l_i+1)}_{(l_i,\theta_v,\theta_v)} > 0$, $p^{(l_i-1)}_{(l_i,\theta_v,\theta_v)} > 0$, and $p^{l_i}_{(l_i,\theta_v,\theta_v)} > 0$, where $\vec{k} \in \mathcal{S}_{Q_i} \times \mathcal{S}^{\vec{i}}_{\theta_v}$. This is true from (6), since $p^{l_i}_{\theta_v} > 0$, and we have $p^{(l_i,l_i+1)}_{(\theta_v,\theta_v)} > 0$, $p^{(l_i,l_i-1)}_{(\theta_v,\theta_v)} > 0$, and $p^{(l_i,l_i)}_{(\theta_v,\theta_v)} > 0$ based on (16).
   - Then, we will prove that $p^{\vec{k}}_{\vec{l},\vec{k}} > 0$. Since $A_{i,t} = k_i - \max[0, k_i - R_{l_i}\Delta T] \geq 0$, we have $p^{k_i}_{l_i,k_i} > 0$ from (4) and $p^{\vec{k}}_{\vec{l},\vec{k}} > 0$ from (5).
   - Therefore, we have $p^{(\{l_i+1\}_{i\in\mathcal{D}},\vec{k})}_{(\vec{l},\vec{k})} > 0$, $p^{(\{l_i-1\}_{i\in\mathcal{D}},\vec{k})}_{(\vec{l},\vec{k})} > 0$ and $p^{(\vec{l},\vec{k})}_{(\vec{l},\vec{k})} > 0$ from (3), and there exists a multi-transition path from $(\vec{l},\vec{k})$ to $(\vec{l^*},\vec{k})$ as $(\vec{l},\vec{k}) \rightarrow (\{l_i+1\}_{i\in\mathcal{D}},\vec{k}) \rightarrow \ldots \rightarrow (\{l_i^*-1\}_{i\in\mathcal{D}},\vec{k}) \rightarrow (\vec{l^*},\vec{k})$ or $(\vec{l},\vec{k}) \rightarrow (\{l_i-1\}_{i\in\mathcal{D}},\vec{k}) \rightarrow \ldots \rightarrow (\{l_i^*+1\}_{i\in\mathcal{D}},\vec{k}) \rightarrow (\vec{l^*},\vec{k})$, where the probability of each transition is non-zero.
2) $(\vec{l^*},\vec{k}) \longrightarrow (\vec{l^*},\vec{h})$.
   - First, we will prove that $p^{\vec{h}}_{\vec{l^*},\vec{k}} > 0$. Since $A_{i,t} = h_i - \max[0, k_i - R_{l_i^*}\Delta T] \geq 0$ when $R_{l_i^*}\Delta T \geq k_i$, we have $p^{h_i}_{l_i^*,k_i} > 0$ from (4) and $p^{\vec{h}}_{\vec{l^*},\vec{k}} > 0$ from (5).
   - Then, we will prove that $p^{\vec{l^*}}_{\vec{l^*},\vec{k},\vec{h}} > 0$. From (23), we only need to prove that $p^{l_i^*}_{(l_i^*,\vec{k},\vec{h})} > 0$. According to Theorem 1, this is equivalent to proving that $p^{l_i^*}_{(l_i^*,\theta_v,\theta_w)} > 0$, where $\vec{k} \in \mathcal{S}_{Q_i} \times \mathcal{S}^{\vec{i}}_{\theta_v}$ and $\vec{h} \in \mathcal{S}_{Q_i} \times \mathcal{S}^{\vec{i}}_{\theta_w}$. Since $\pi_{l_i^*|\theta_v} > 0$ and from (6), we need to prove that $p^{l_i^*,l_i^*}_{(\theta_v,\theta_w)} > 0$. According to (17), since we have proved that $p^{(l_i^*,l_i^*+1)}_{(\theta_v,\theta_v)} > 0$, $p^{(l_i^*,l_i^*-1)}_{(\theta_v,\theta_v)} > 0$, and $p^{(l_i^*,l_i^*)}_{(\theta_v,\theta_v)} > 0$ in the above discussion, we only need to show that at least one of three probabilities $\hat{p}^{l_i}_{(l_i^*+1,\theta_v,\theta_w)}$, $\hat{p}^{l_i^*}_{(l_i^*-1,\theta_v,\theta_w)}$, and $\hat{p}^{l_i^*}_{(l_i^*,\theta_v,\theta_w)}$ is non-zero. From Lemma 1, we have $\hat{p}^{l_i^*}_{(l_i^*,\theta_v,\theta_w)}$ is always non-zero irrespective of the relationship between θ_v and θ_w. Therefore, we can prove that $p^{\vec{l^*}}_{\vec{l^*},\vec{k},\vec{h}} > 0$.
   - Therefore, the transition from $(\vec{l^*},\vec{k})$ to $(\vec{l^*},\vec{h})$ has non-zero probability from (3).
3) $(\vec{l^*},\vec{h}) \longrightarrow (\vec{n},\vec{h})$. The proof is the same with (1).

Combining (1), (2) and (3), we can prove that there exits a multi-transition path with non-zero probability from state $(\vec{l},\vec{k})$ to $(\vec{n},\vec{h})$, i.e, $(\vec{l},\vec{k}) \longrightarrow (\vec{l^*},\vec{k}) \rightarrow (\vec{l^*},\vec{h}) \longrightarrow (\vec{n},\vec{h})$, where $R_{l_i^*}\Delta T \geq k_i$. Since $K \leq R_L \Delta T$, there always exists such l_i^* that satisfies this condition. ■

Lemma 3: The Markov chain $(\vec{H}_t, \vec{Q}_t)$ is homogeneous and positive recurrent, if $K \leq R_L \Delta T$.

Proof: Since the transition probability matrix $\mathbf{P}$ is independent of the time slot t, the Markov chain is homogeneous [34]. From Theorem 3.3 in [34], $(\vec{H}_t, \vec{Q}_t)$ is positive recurrent, since it has finite state space $(L\times(K+1))^D$ and is irreducible from Lemma 2. ■

From Theorem 3.1 in [34], Theorem 3 is valid if and only if the Markov chain $(\vec{H}_t, \vec{Q}_t)$ is irreducible, homogeneous and positive recurrent, which have been proved in Lemma 2 and Lemma 3.

C. Convergence of the fixed point iteration

According to Theorem 2 in [23], in order to prove the convergence of the fixed point iteration for the decomposed DSPN model as described in (17), it is sufficient to show that the following lemma is true.

Lemma 4: The Markov chain $(H_{i,t}, Q_{i,t})$ corresponding to the ith subsystem in the decomposed model is irreducible, if $K \leq R_L \Delta T$.

Proof: Similar to the proof of Lemma 2, we can prove Lemma 4 by showing that for each transition from state (l_i,k_i) to (n_i,h_i), there exists a multi-transition path with non-zero probability, which is denoted as $(l_i,k_i) \longrightarrow (n_i,h_i)$. Comparing Lemma 4 with Lemma 2, we can prove that there is a multi-transition path $(l_i,k_i) \longrightarrow (l_i^*,k_i) \rightarrow (l_i^*,h_i) \longrightarrow (n_i,h_i)$, where $R_{l_i^*}\Delta T \geq k_i$, if we prove that $\widetilde{p}^{l_i+1}_{(l_i,k_i,k_i)} > 0$, $\widetilde{p}^{l_i-1}_{(l_i,k_i,k_i)} > 0$, $\widetilde{p}^{l_i}_{(l_i,k_i,k_i)} > 0$ and $\widetilde{p}^{l_i^*}_{(l_i^*,k_i,h_i)} > 0$. This is true

by (26), since we have proved that $p^{(l_i+1)}_{(l_i,\vec{k},\vec{k})} > 0$, $p^{(l_i-1)}_{(l_i,\vec{k},\vec{k})} > 0$, $p^{l_i}_{(l_i,\vec{k},\vec{k})} > 0$, and $p^{l_i^*}_{(l_i^*,\vec{k},\vec{h})} > 0$ in Lemma 2, and we also have $\pi_{k_j,h_j} \geq 0$ for any $k_j, h_j \in \mathcal{S}_{Q_j}$, $j \in \mathcal{D}\backslash\{i\}$ and $\sum_{\substack{\{k_j\}_{j\in\mathcal{D}\backslash\{i\}}\in\mathcal{S}^{\bar{i}}_Q \\ \{h_j\}_{j\in\mathcal{D}\backslash\{i\}}\in\mathcal{S}^{\bar{i}}_Q}} \prod_{j\in\mathcal{D}\backslash\{i\}} \pi_{k_j,h_j} = 1$. ■

REFERENCES

[1] L. Lei, Z. Zhong, C. Lin, and X. Shen, "Operator controlled device-to-device communications in LTE-advanced networks," *IEEE Wireless Mag.*, vol. 19, no. 3, pp. 96–104, June 2012.

[2] G. Fodor, E. Dahlman, G. Mildh, S. Parkvall, N. Reider, G. Miklos, and Z. Turanyi, "Design aspects of network assisted device-to-device communications," *IEEE Commun. Mag.*, vol. 50, no. 3, pp. 170–177, Mar. 2012.

[3] M. S. Corson, R. Laroia, J. Li, V. Park, T. Richardson, and G. Tsirtsis, "Toward proximity-aware internetworking," *IEEE Wireless Mag.*, vol. 17, no. 6, pp. 26–33, Dec. 2010.

[4] K. Doppler, M. Rinne, C. Wijting, C. B. Ribeiro, and K. Hugl, "Device-to-device communication as an underlay to LTE-Advanced Networks," *IEEE Commun. Mag.*, vol. 47, no. 12, pp. 42–49, Dec. 2009.

[5] C.-H. Yu, K. Doppler, C. B. Ribeiro, and O. Tirkkonen, "Resource sharing optimization for device-to-device communication underlaying cellular networks," *IEEE Trans. Wireless Commun.*, vol. 10, no. 8, pp. 2752–2763, Aug. 2011.

[6] X. Wu *et al.*, "FlashLinQ: a synchronous distributed scheduler for peer-to-peer ad hoc networks," in *2010 Allerton Conf.*.

[7] H. Wang and X. Chu, "Distance-constrained resource-sharing criteria for device-to-device communications underlaying cellular networks," *Electron. Lett.*, vol. 48, no. 9, pp. 528–530, Apr. 2012.

[8] M. Jung, K. Hwang, and S. Choi, "Joint mode selection and power allocation scheme for power-efficient device-to-device (D2D) communication," in *2012 IEEE Veh. Technol. Conf. – Spring*.

[9] M. Zulhasnine, C. Huang, and A. Srinivasan, "Efficient resource allocation for device-to-device communication underlaying LTE network," in *Proc. 2010 IEEE Wireless Commun. Netw. Conf.*

[10] H. Xing and S. Hakola, "The investigation of power control schemes for a device-to-device communication integrated into OFDMA cellular system," in *2010 IEEE International Symp. Personal Indoor Mobile Radio Commun.*

[11] C.-H. Yu, O. Tirkkonen, K. Doppler, and C. Ribeiro, "Power optimization of device-to-device communication underlaying cellular communication," in *2009 IEEE International Conf. Commun.*

[12] G. Fayolle and R. Iasnogorodski, "Two coupled processors: the reduction to a Riemann-Hilbert problem," *Z. Wahr. verw. Geb.*, vol. 47, pp. 324–351, 1979.

[13] A. G. Konheim, I. Meilijson, and A. Melkman, "Processor-sharing of two parallel lines," *J. Appl. Probab.*, vol. 18, no. 4, pp. 952–956, 1981.

[14] F. Guillemin and D. Pinchon, "Analysis of generalized processor-sharing systems with two classes of customers and exponential services," *J. Appl. Probab.*, vol. 41, no. 3, pp. 832–858, 2004.

[15] T. Bonald, S. Borst, N. Hegde, and A. Proutiere, "Wireless data performance in multi-cell scenarios," in *Proc. 2004 ACM Sigmetrics*.

[16] T. Bonald, S. Borst, and A. Proutiere, "Inter-cell scheduling in wireless data networks," in *2005 European Wireless Conf.*

[17] B. Rengarajan, C. Caramanis, and d. G. Veciana, "Analyzing queuing systems with coupled processors through semdefinite programming." Available: http://users.ece.utexas.edu/∼gustabo/papers/SdpCoupledQs.pdf, 2008.

[18] Rengarajan B. and Veciana d. G, "Practical adaptive user association policies for wireless systems with dynamic interference," *IEEE/ACM Trans. Netw.*, vol. 19, no. 6, pp. 1690–1703, Dec. 2011.

[19] H. S. Wang and N. Moayeri, "Finite-state Markov channel—a useful model for radio communication channels," *IEEE Trans. Veh. Technol.*, vol. 44, pp. 163–171, Feb. 1995.

[20] 3GPP TS 36.213, V10.3.0, "Technical specification group radio access network; Evolved Universal Terrestrial Radio Access; Physical Layer Procedures (Release 10)," 2011.

[21] Q. Liu, S. Zhou, and G. B. Giannakis, "Queueing with adaptive modulation and coding over wireless links: cross-layer analysis and design," *IEEE Trans. Wireless Commun.*, vol. 50, no. 3, pp. 1142–1153, May 2005.

[22] G. Ciardo and K. S. Trivedi, "A decomposition approach for stochastic reward net models," *Performance Evaluation*, vol. 18, pp. 37–59, 1993.

[23] V. Mainkar and K. S. Trivedi, "Fixed point iteration using stochastic reward nets," in *Proc 1995 International Workshop Petri Nets Performance Models*, pp. 21–30.

[24] L. Lei, C. Lin, J. Cai, and X. Shen, "Performance analysis of opportunistic wireless schedulers using stochastic Petri nets," *IEEE Trans. Wireless Commun.*, vol. 7, no. 4, pp. 5461–5472, Apr. 2009.

[25] R. Schoenen, A. B. Sediq, H. Yanikomeroglu, G. Senarath, and Z. Chao, "Spectral efficiency and fairness tradeoffs in cellular networks with realtime-nonrealtime traffic mix using stochastic Petri nets," in *Proc. 2012 IEEE VTC – Fall*.

[26] R. Schoenen, M. Salem, A. Sediq, and H. Yanikomeroglu, "Multihop wireless channel models suitable for stochastic Petri nets and Markov state analysis," in *Proc. 2011 IEEE VTC – Spring*.

[27] S. Geetha and R. Jayaparvathy, "Modeling and analysis of bandwidth allocation in IEEE 802.16 MAC: a stochastic reward net approach," *Int. J. Commun., Netw. Syst. Sciences*, vol. 3, no. 7, pp. 631–637, July 2010.

[28] A. S. Miner, G. Ciardo, and S. Donatelli, "Using the exact state space of a Markov model to compute approximate stationary measures," in *Proc. 2000 ACM SIGMETRICS*, pp. 207–216.

[29] M. Wan, G. Ciardo, and A. S. Miner, "Approximate steady-state analysis of large Markov models based on the structure of their decision diagram encoding," *Performance Evaluation*, vol. 68, no. 5, pp. 463–486, May 2011.

[30] L. Lei, Y. Han, Z. Zhong, and C. Lin, "Performance analysis of device-to-device communications with frequency reuse using stochastic Petri nets," *2013 IEEE ICC*.

[31] L. Le and E. Hossain, "Tandem queue models with applications to QoS routing in multihop wireless networks," *IEEE Trans. Mobile Comput.*, vol. 7, no. 8, Aug. 2008.

[32] "Selection procedures for the choice of radio transmission technologies of the UMTS," 3GPP TR 30.03U, version 3.2.0, 1998.

[33] ITU-R M.1225, "Guidelines for the Evaluation of Radio Transmission Technologies (RTTs) for IMT-2000," 1997.

[34] P. Bremaud, *Markov Chains: Gibbs Fields, Monte Carlo Simulation, and Queues*. Springer-Verlag, 1999.

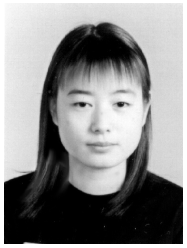

Lei Lei received a B.S. degree in 2001 and a PhD degree in 2006, respectively, from Beijing University of Posts & Telecommunications, China, both in telecommunications engineering. From July 2006 to March 2008, she was a postdoctoral fellow at Computer Science Department, Tsinghua University, Beijing, China. She worked for the Wireless Communications Department, China Mobile Research Institute from April 2008 to August 2011. She has been an Associate Professor with the School of Electronic and Information Engineering, Beijing Jiaotong University, since Sept. 2011. Her current research interests include performance evaluation, quality-of-service and radio resource management in wireless communication networks.

Yingkai Zhang received his B.S. degree in Beijing University of Posts and Telecommunications (BUPT), China, in 2011. He is currently studying for a master's degree in the School of Information and Communication Engineering, BUPT. His research interests lie in wireless communications, especially radio resource management and device-to-device communications.

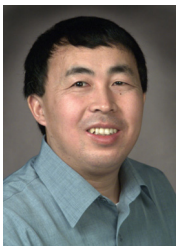

Xuemin (Sherman) Shen (IEEE M'97-SM'02-F09) received the B.Sc.(1982) degree from Dalian Maritime University (China) and the M.Sc. (1987) and Ph.D. degrees (1990) from Rutgers University, New Jersey (USA), all in electrical engineering. He is a Professor and University Research Chair, Department of Electrical and Computer Engineering, University of Waterloo, Canada. He was the Associate Chair for Graduate Studies from 2004 to 2008. Dr. Shen's research focuses on resource management in interconnected wireless/wired networks, wireless network security, wireless body area networks, vehicular ad hoc and sensor networks. He is a co-author/editor of six books, and has published more than 600 papers and book chapters in wireless communications and networks, control and filtering. Dr. Shen served as the Technical Program Committee Chair for IEEE VTC'10 Fall, the Symposia Chair for IEEE ICC'10, the Tutorial Chair for IEEE VTC'11 Spring and IEEE ICC'08, the Technical Program Committee Chair for IEEE Globecom'07, the General Co-Chair for Chinacom'07 and QShine'06, the Chair for IEEE Communications Society Technical Committee on Wireless Communications, and P2P Communications and Networking. He also serves/served as the Editor-in-Chief for *IEEE Network*, *Peer-to-Peer Networking and Application*, and *IET Communications*; a Founding Area Editor for IEEE TRANSACTIONS ON WIRELESS COMMUNICATIONS; an Associate Editor for IEEE TRANSACTIONS ON VEHICULAR TECHNOLOGY, *Computer Networks*, and *ACM/Wireless Networks*, etc.; and the Guest Editor for IEEE JSAC, *IEEE Wireless Communications*, *IEEE Communications Magazine*, and *ACM Mobile Networks and Applications*, etc. Dr. Shen received the Excellent Graduate Supervision Award in 2006, and the Outstanding Performance Award in 2004, 2007 and 2010 from the University of Waterloo, the Premier's Research Excellence Award (PREA) in 2003 from the Province of Ontario, Canada, and the Distinguished Performance Award in 2002 and 2007 from the Faculty of Engineering, University of Waterloo. Dr. Shen is a registered Professional Engineer of Ontario, Canada, an IEEE Fellow, an Engineering Institute of Canada Fellow, and a Distinguished Lecturer of IEEE Vehicular Technology Society and Communications Society.

Chuang Lin is a professor of the Department of Computer Science and Technology, Tsinghua University, Beijing, China. He is a Honorary Visiting Professor, University of Bradford, UK. He received the Ph.D. degree in Computer Science from the Tsinghua University in 1994. His current research interests include computer networks, performance evaluation, network security analysis, and Petri net theory and its applications. He has published more than 500 papers in research journals and IEEE conference proceedings in these areas and has published five books.

Professor Lin is a senior member of the IEEE. He serves as the Technical Program Vice Chair, the 10th IEEE Workshop on Future Trends of Distributed Computing Systems (FTDCS 2004); the General Chair, ACM SIGCOMM Asia workshop 2005 and the 2010 IEEE International Workshop on Quality of Service (IWQoS 2010); the Associate Editor, IEEE TRANSACTIONS ON VEHICULAR TECHNOLOGY; and the Area Editor, *Journal of Computer Networks*.

Zhangdui Zhong received the B.Eng. and M.Sc. degrees from Northern Jiaotong University (currently Beijing Jiaotong University), Beijing, China, in 1983 and 1988, respectively.

He has been a Professor with the School of Electronic and Information Engineering, Beijing Jiaotong University, since 2000. He is now a director of School of Computer and Information Technology and a Chief Scientist of State Key Laboratory of Rail Traffic Control and Safety in Beijing Jiaotong University. He is also a director of the Innovative Research Team of Ministry of Education, and a Chief Scientist of Ministry of Railways in China. He has authored seven books and over 200 technical papers in the field of wireless communication. His current research interests include wireless communication theory for railway systems, wireless ad hoc networks, channel modeling, radio resource management, intelligent transportation systems, and GSM-R systems.